The influence of anchoring group position in ruthenium dye molecule on performance of dye-sensitized solar cells.

Maciej Zalas[1,2,3]*, Błażej Gierczyk[1], Alberto Bossi[3,4], Patrizia Romana Mussini[2], Maciej Klein[5,6], Radosław Pankiewicz[1], Małgorzata Makowska-Janusik[7], Łukasz Popenda[8] and Waldemar Stampor[5].

[1] Adam Mickiewicz University in Poznań, Faculty of Chemistry, Umultowska 89 B, 61-614 Poznań, Poland

[2] Department of Chemistry, University of Milan, Via Golgi 19, 20133 Milano, Italy

[3] SmartMatLab Centre, Via Golgi 19, 20133 Milano, Italy

[4] Istituto di Scienze e Tecnologie Molecolari – CNR, via Fantoli 16/15, 20138 Milano, Italy.

[5] Department of Physics of Electronic Phenomena, Faculty of Applied Physics and Mathematics, Gdansk University of Technology, Narutowicza 11/12, 80-233 Gdansk, Poland

[6] Distributed Energy Department, The Szewalski Institute of Fluid-Flow Machinery, Polish Academy of Sciences, Fiszera 14, 80-231 Gdansk, Poland

[7] Institute of Physics, Faculty of Mathematics and Natural Science, Jan Dlugosz University, Al. Armii Krajowej 13/15, 42-200 Częstochowa, Poland

[8] NanoBioMedical Centre, Adam Mickiewicz University in Poznań, Umultowska 85, 61-614 Poznań, Poland

*corresponding author, address: Adam Mickiewicz University in Poznań, Faculty of Chemistry, Umultowska 89 B, 61-614 Poznań, Poland, phone: 0048618291708, fax: 0048618291505, email: maciej.zalas@amu.edu.pl

Keywords:

Ruthenium sensitizers, anchoring group position, dye-sensitized solar cells, electron injection efficiency,

Abstract

The effect of anchoring group position and, in consequence, the orientation of the ruthenium dye molecule on titania surface on the performance of dye-sensitized solar cells has been studied intensively. Three model ruthenium sensitizing dyes bearing carboxylic anchoring group in *ortho*, *meta* or *para* position were synthesized and well characterized by spectroscopic, electrochemical, photophysical and photochemical measurements. The results were confronted with the quantum-mechanical calculations and discussed. The *para* derivative has been found as the most effective sensitizer with the cells efficiency twice higher than the *meta* and four times higher than the *ortho* derivatives.

1. Introduction

Dye-sensitized solar cells (DSSCs) seem to be promising devices efficiently converting sunlight to electricity, because of their relatively high efficiency, simple fabrication methods and low cost of production [1-4]. Typical DSSC is composed of dye-sensitized nanocrystalline semiconducting oxide, liquid or solid electrolyte and a counter electrode, but the dye is one of the most important component and is often called "the heart of the system" which indicates its key role in determination of the device photovoltaic performance. The initial types of DSSCs based on a combination of mesoporous titania sensitized with ruthenium complex cooperating with iodine-based electrolytes permitted the efficiencies up to 11.9%, but the devices of this kind, up to now, have never surpassed the efficiency level of about 12% and the recent record is 12.3% [5, 6]. Further application of the new type of organic donor-π-acceptor dyes based on

porphyrin with cobalt-based redox mediators permitted obtaining efficiencies over 13% and still has much potential of development [7-10].

Ruthenium sensitizers development is focused on structural modification of the ancillary ligands to improve electron injection efficiency, light harvesting and, in consequence, the performance of DSSCs. Modification of anchoring ligands is performed very seldom and only a few papers have been published in this area. Funaki et al. have synthesized the "black dye" analogues with π-expanded terpyridine ligand having phenylene-ethynylene chains and the anchoring carboxyl group shifted to the end of expanding chain [11]. They found that the longer the phenylene-ethynylene chain the lower the efficiency of the cell and explained this phenomenon by the aggregation of the dye molecules on the electrode surface. The improvement in the cells efficiencies sensitized by a "black dye" with the anchoring chain modified by cyanoacetic acid-2-thienyl moiety, have been reported by Vincent Joseph et al. [12].

In our previous work we investigated the dinuclear ruthenium bipyridine complex B1 with dendritic anchoring ligand [13, 14]. The B1 dye was less active in the cell conditions than its commercially available mononuclear analogue. One of possible reasons for relatively poor performance of B1 dye, proposed by us, was the *meta* position of the carboxylic anchoring group in relation to the ruthenium bipyridine complex moieties that may lead to poor electronic communication with the TiO_2 orbitals. Previously published papers clearly indicate that the *meta* position of the anchoring group in the ruthenium dye molecule results in lower efficiency of the sensitized cells [15-17]. However, the hitherto literature on the subject has been focused on the dyes with at least two anchors in one molecule and the *meta* location triggers competing reactions and steric problems during the dye adsorption process. Moreover, Hart et al. have investigateed the effect of anchoring group position in the porphyrin sensitizers with only one anchoring group and they found that the *meta* position is the most effective in electron injection

process and, in consequence, gives more effective cells [18], but further investigations of other groups have strongly refute these findings [19, 20].

In this work, we do not aim at reaching the next DSSC efficiency record but we try to find the answer to the fundamental question on the effect of the position of a single anchoring group on the overall photon-to-current efficiency of the cell. Therefore, in order to better understand the electron transfer process between the dye molecule and the titania electrode three model-dyes, each of them with only one anchoring group, already known *para* [21] and two new *meta* and *ortho*, have been synthetized and examined by electrochemical, photophysical and photochemical techniques as well as density functional theory (DFT) calculations. Solar cells with the *para* derivative as a sensitizer exhibit the highest performance with the photoconversion efficiency twice higher than the *meta* derivatives and four times higher than the *ortho* ones.

2. Experimental

2.1. Synthesis

The compound 4-bromo-2,2'-bipyridine and 4-ethynyl-2,2'-bipyridine was obtained by published methods [14, 22], other compounds were commercial products (Sigma-Aldrich, USA).

Ethyl ethynylbenzoates (**2**)

A solution of corresponding ethyl bromobenzoate (5.00 g; 22 mmol) and trimethylsilylacetylene (15 mL; 108 mmol) in triethylamine (80 mL) was deoxygenated and 200 mg of $Pd_2(dba)_3$, 300 mg of triphenylphosphine and 50 mg of cooper(I) iodide were added. The mixture obtained was stirred under argon at 353 K, over 24 h, then the solvent was evaporated, the residue was mixed with 5% HCl (200 mL) and the product was extracted with diethyl ether (2×100 mL). The organic layer was washed with water, dried over Na_2SO_4 and

evaporated. The crude trimethylsilyl derivative **1** was dissolved in freshly distilled THF (100 ml), then 1.25 mL of glacial acetic (22 mmol) acid and solution of 7.15 g (23 mmol) of tetrabutylammonium fluoride trihydrate in 20 mL of THF was added. The mixture was allowed to react over 0.5 h, the solvent was evaporated and the product was purified by column chromatography (SiO$_2$; hexane/dichloromethane, 2:1 v/v).

m-2: Yellowish brown crystals; m.p. ~293 K. Yield: 90% (3.45 g). ^{1}H NMR (CDCl$_3$): δ 8.17 (d, 1H; 1.4 Hz), 8.02 (dt, 1H; 7.7 & 1.4 Hz), 7.66 (dt, 1H; 7.7 & 1.4 Hz), 7.41 (t, 1H; 7.7 Hz), 4.39 (q, 2H; 7.3 Hz), 3.12 (s, 1H), 1.41 (t, 3H; 7.3 Hz). HRMS: 174.0680 (calc. for C$_{11}$H$_{10}$O$_2$: 174.0681). ^{13}C NMR (CDCl$_3$): δ 165.5, 136.9, 132.7, 131.7, 130.9, 129.8, 128.7, 82.3, 81.1, 61.2, 14.1.

p-2: Yellowish brown crystals; m.p. ~293 K. Yield: 94% (3.60 g). ^{1}H NMR (CDCl$_3$): δ 8.00 (*pseudo*d, 2H), 7.55 (*pseudo*d, 2H), 4.38 (q, 2H; 7.3 Hz), 3.22 (s, 1H), 1.40 (t, 3H; 7.3 Hz). HRMS: 174.0677 (calc. for C$_{11}$H$_{10}$O$_2$: 174.0681). ^{13}C NMR (CDCl$_3$): δ 165.9, 132.0, 130.4, 129.4, 126.6, 82.8, 79.9, 61.1, 14.2.

Ethyl (2-(2,2'-bipyridin-4-yl)ethynyl)benzoates (**3**)

1.00 g of corresponding ethyl ethynylbenzoate (5.7 mmol) and 1.40 g of 4-bromo-2,2'-bipyridine (6.4 mmol) was dissolved in 60 mL of deoxygenated triethylamine and 100 mg of Pd$_2$(dba)$_3$, 150 mg of triphenylphosphine and 30 mg of cooper(I) iodide were added. The mixture obtained was heated under argon over 24 h. After that the solvent was evaporated, the product was extracted with chloroform and recrystallized from methanol.

m-3: Dirty yellow flocks; m.p. 438-441 K. Yield: 85% (1.59 g). ^{1}H NMR (CDCl$_3$): δ 8.71 (bs, 2H), 8.57 (bs; 1H), 8.43 (bs, 1H), 8.24 (t, 1H; 1.6 Hz), 8.06 (dt, 1H; 7.8 & 1.4 Hz), 7.84 (t, 1H; 7.5 Hz), 7.73 (dt, 1H; 7.8 & 1.4 Hz), 7.47 (t, 1H; 7.8 Hz), 7.42 (bs, 1H), 7.35 (bs, 1H), 4.41 (q, 2H; 7.2 Hz), 1.43 (t, 3H; 7.2 Hz). ^{13}C NMR (CDCl$_3$): δ 165.7, 156.1, 155.3, 149.1, 137.0, 135.8,

133.0, 132.1, 131.0, 130.0, 128.6, 125.3, 124.1, 123.3, 122.6, 121.2, 92.8, 87.8, 61.3, 14.3. HRMS: 328.1205 (calc. for $C_{21}H_{16}N_2O_2$: 328.1212).

p-3: Dirty yellow flocks; m.p. 453-455 K. Yield: 87% (1.63 g). ^{1}H NMR ($CDCl_3$): δ 8.71 (bs, 1H), 8.68 (bs, 1H), 8.56 (bs, 1H), 8.42 (d, 1H; 8.0 Hz), 8.06 (*pseudo*d, 2H), 7.83 (td, 1H; 7.7 & 1.6 Hz), 7.62 (*pseudo*d, 2H), 7.40 (d, 1H; 4.6 Hz), 7.34 (dd, 1H; 6.8 & 5.0 Hz), 4.40 (q, 2H; 7.1 Hz), 1.41 (t, 3H; 7.1 Hz). ^{13}C NMR ($CDCl_3$): δ 165.8, 156.2, 155.3, 149.2, 137.0, 131.8, 131.7, 130.6, 129.5, 126.6, 125.2, 124.1, 123.2, 121.2, 92.8, 89.5, 61.2, 14.3. HRMS: 328.1217 (calc. for $C_{21}H_{16}N_2O_2$: 328.1212).

(2-(2,2'-Bipyridin-4-yl)ethynyl)benzoic acids (***m*-4, *p*-4; Lm, Lp**)

1.00 g of **3** (3 mmol) was dissolved in 150 mL of THF and 100 mL of methanol. To the solution obtained 0.5 g of lithium hydroxide (21 mmol) in 25 mL of water was added. The mixture was stirred overnight at room temperature, the solvent was evaporated and the solid residue was suspended in water (50 mL). The solution was neutralized with 10% HCl and the precipitated product was filtered off, washed with water and dried.

m-4 (**Lm**): Yellowish powder; m.p. 496 K. Yield: 95% (0.86 g). ^{1}H NMR (DMSO-d_6): δ 11.3 (bs, 1H), 8.73 (dd, 1H; 4.9 & 0.8 Hz), 8.71 (dd, 1H; 4.7, 1.9 & 1.0 Hz), 8.45 (dd, 1H; 1.7 & 1.0 Hz), 8.38 (dd, 1H; 7.9 & 1.0 Hz), 8.10 (td, 1H; 1.7 & 0.8 Hz), 7.98 (td, 1H; 7.7 & 1.7), 7.95 (dt, 1H; 7.6 & 1.3 Hz), 7.60 (m, 2H), 7.50 (ddd, 1H; 7.5, 4.8 & 1.0 Hz), 7.40 (t, 1H; 7.6 Hz). ^{13}C NMR (DMSO-d_6): δ 168.3, 155.6, 154.3, 149.8, 149.4, 140.8, 137.5, 132.5, 132.0, 131.5, 130.4, 127.9, 125.4, 124.6, 121.9, 120.6, 120.0, 94.4, 86.2. HRMS: 300.0891 (calc. for $C_{19}H_{12}N_2O_2$: 300.0899).

p-4 (**Lp**): Yellowish powder; m.p. 518-524 K. Yield: 97% (0.87 g). ^{1}H NMR (DMSO-d_6): δ 11.0 (bs, 1H), 8.73 (dd, 1H; 4.9 & 0.8 Hz), 8.71 (ddd, 1H; 4.7, 1.8 & 0.9 Hz), 8.45 (dd, 1H; 1.6 & 0.8 Hz), 8.39 (dt, 1H; 7.9 & 1.1 Hz), 7.98 (ddd, 1H; 7.9, 7.7 & 1.6 Hz), 7.92 (*pseudo*d, 2H),

7.59 (dd, 1H; 5.0 & 1.8 Hz), 7.57 (*pseudo*d, 2H), 7.50 (ddd, 1H; 7.4, 4.7 & 1.2 Hz). ^{13}C NMR (DMSO-d$_6$): δ 168.6, 155.6, 154.3, 149.8, 149.4, 141.5, 137.5, 131.5, 130.9, 129.3, 125.4, 124.7, 121.9, 121.2, 120.6, 94.3, 87.2. HRMS: 300.0888 (calc. for C$_{19}$H$_{12}$N$_2$O$_2$: 300.0899).

2-Bromobenzoic acid trimethylsilyl ester (5)

2-Bromobenzoic acid (5.00 g; 25 mmol) was dissolved in dry dichloromethane (100 mL) and 26 mg of sodium saccharinate (0.125 mmol) was added. The mixture was heated under reflux in inert atmosphere and the hexamethyldisilazane (3.23 g, 20 mmol) was added dropwise over 5 min. After 2 h the mixture was filtered and the solvent and excess of silanizing agent were evaporated in vacuum. The crude product was obtained as colorless liquid (6.63 g; yield: 98%), readily hydrolyzing on air. ^{1}H NMR (CDCl$_3$): δ 7.87 (dd, 1H; 7.7 & 1.8 Hz), 7.65 (d, 1H; 7.7 Hz), 7.35 (t, 1H; 7.7 Hz), 7.31 (td, 1H; 7.7 & 1.8 Hz). HRMS: 271.9860 (calc. for C$_{10}$H$_{13}$BrO$_2$Si: 271.9868).

2-(2-(2,2'-Bipyridin-4-ylethynyl)benzoic) acid (o-4; Lo)

1.50 g (5.5 mol) of protected 2-bromobenzoic acid (5) was dissolved in mixture of 50 mL of anhydrous triethylamine with 30 mL anhydrous toluene and 1 g (2.2 mmol) of 4-ethynyl-2,2'-bipyridine was added. After adding of the catalysts (150 mg of Pd$_2$(dba)$_3$, 300 mg of PPh$_3$ and 75 mg of CuI) the mixture was heated at 353 K over 24 h. After that the solvent was evaporated and the mixture was stirred with water over 1 h. The product was filtered off and purified by column chromatography (SiO$_2$; CH$_2$Cl$_2$/Et$_2$O, 1:1 v/v) to obtain 0.49 g (75%) of yellowish powder. ^{1}H NMR (DMSO-d$_6$): δ 8.81 (dd, 1H; 4.9 & 0.9 Hz), 8.74 (ddd, 1H; 4.7, 1.8 & 0.9 Hz), 8.51 (dd, 1H; 1.7 & 0.9 Hz), 8.41 (dt, 1H; 7.9 & 1.1 Hz), 8.00 (td, 1H; 7.7 & 1.8 Hz), 7.81 (m, 2H), 7.72 (dd, 1H; 4.9 & 1.6 Hz), 7.52 (ddd, 1H; 7.5, 4.6 & 1.1 Hz), 7.48 (m, 2H). HRMS: 300.0907 (calc. for C$_{19}$H$_{12}$N$_2$O$_2$: 300.0899).

Bis(2,2'-bipyridine)(4-(2-(carboksyphenyl)ethynyl)-2,2'-bipyridine)ruthenium(II)

hexafluorophosphate(V) (**6; RuLomp**)

1.00 g of **4** (3.3 mmol) and 1.74 g of bis(2,2'-bipyridine)ruthenium dichloride dihydrate (3.3 mmol) were dissolved in anhydrous ethanol (200 mL) and the resulting solution was refluxed over 10 h under argon in dark. After that the insoluble byproducts were filtered off and the solvent was evaporated. The obtained solid was dissolved in methanol (15 mL) and the solution was filtered. To the obtained mixture a solution of ammonium hexafluorophosphate(V) in water (2 g in 4 mL) was added. The formed precipitate was filtered off, dissolved in methanol (15 mL) and the precipitation procedure with NH_4PF_6 solution was repeated. The final product was filtered, washed with water and diethyl ether and dried in vacuum.

***o*-6** (**RuLo**): Red amorphous solid. Yield: 77% (2.57 g). ^{1}H NMR (CD$_3$CN): δ 8.73 (d, 1H; 5.1 Hz), 8.68 (d, 1H; 4.2 Hz), 8.64 (dd, 1H; 1.4 & 0.9 Hz), 8.52 (m, 4H), 8.44 (d, 1H; 7.8 Hz), 8.07 (m, 4H), 7.92 (td, 1H; 7.8 & 1.8 Hz), 7.76 (m, 3H), 7.70 (m, 4H), 7.53 (dd, 1H; 4.9 & 1.6 Hz), 7.42 (m, 6H), 5.9 (bs, 1H). ^{13}C NMR (CD$_3$CN): δ 168.8, 158.5, 157.8 (×3), 157.7, 157.2, 155.6, 152.8, 152.7, 152.6, 152.5, 150.7, 150.3, 138.9 (×3), 138.3, 130.8, 130.3, 130.2, 130.0, 128.6 (×2), 128.5, 127.6, 126.9, 125.5, 125.3, 123.9, 121.8, 83.6, 80.8. Anal.: C 46.77%, H 2.85%, N 8.20% (calc. for $C_{39}H_{28}N_6O_2P_2F_{12}Ru$: C 46.67%, H 2.81%, N 8.37%).

***m*-6** (**RuLm**): Red amorphous solid. Yield: 87% (2.91 g). ^{1}H NMR (CD$_3$CN): δ 9.8 (bs, 1H), 8.64 (d, 1H; 1.4 Hz), 8.53 (d, 1H; 8.0 Hz), 8.50 (m, 5H), 8.25 (t, 1H; 1.4 Hz), 8.07 (m, 5H), 7.82 (dt, 1H; 7.8 & 1.3 Hz), 7.80 (d, 1H; 5.6 Hz), 7.75 (d, 1H; 5.6 Hz), 7.73 (m, 4H), 7.57 (t, 1H; 7.6 Hz), 7.46 (dd, 1H; 5.8 & 1.6 Hz), 7.41 (m, 5H). ^{13}C NMR (CD$_3$CN): δ 167.6, 158.5, 157.9, 157.8, 157.5, 152.7, 152.6, 152.5, 138.9 (×2), 138.8, 136.6, 134.0, 133.0, 132.0, 130.2, 129.5, 128.8, 128.6 (×2), 128.5, 126.4, 125.4, 125.2, 122.4, 97.5, 86.8. Anal.: C 46.29%, H

2.63%, N 8.30% (calc. for $C_{39}H_{28}N_6O_2P_2F_{12}Ru$: C 46.67%, H 2.81%, N 8.37%). ESI-MS: 357.0 ($[L_2L'Ru]^{2+}$), 859.0 ($[L_2L'RuPF_6]^+$).

***p*-6** (**RuLp**): Red amorphous solid. Yield: 85% (2.84 g). ^{1}H NMR (CD$_3$CN): δ 8.64 (d, 1H; 1.4 Hz), 8.53 (d, 1H; 7.9 Hz), 8.51 (m, 5H), 8.07 (m, 7H), 7.79 (d, 1H; 5.5 Hz), 7.75 (m, 2H), 7.72 (m, 4H), 7.46 (dd, 1H; 5.8 & 1.7 Hz), 7.41 (m, 5H), 6.4 (bs, 1H). ^{13}C NMR (CD$_3$CN): δ 167.0, 158.4, 157.9, 157.8 (×2), 157.7, 157.5, 138.9 (×2), 138.8, 133.0, 132.7, 130.9, 129.6, 128.8, 128.6 (×2), 128.5, 126.9, 126.4, 125.4, 125.2, 97.2, 88.5. Anal.: C 46.35%, H 2.90%, N 8.27% (calc. for $C_{39}H_{28}N_6O_2P_2F_{12}Ru$: C 46.67%, H 2.81%, N 8.37%). ESI-MS: 357.0 ($[L_2L'Ru]^{2+}$), 859.0 ($[L_2L'RuPF_6]^+$).

2.2. Electrochemical and photophysical studies

The redox properties as well as HOMO and LUMO energy levels of the **RuLomp** dyes were investigated by cyclic voltammetry (CV) in acetonitrile (Aldrich) with 0.1 M tetrabutylammonium hexafluorophosphate (Aldrich) as a supporting electrolyte. To compare and better understand the redox properties of investigated dyes the measurements for published elsewhere B1 dendritic dye [13] and two commercial dyes 455PF6 (Solaronix) and Ru(bpy)$_3$Cl$_2$ (Sigma-Aldrich) were also performed. The Supporting Information includes the CV data for free ligands **Lm** and **Lp** and dendritic **L1** [14] in both free acidic and esterified forms. The electrochemical characterizations were performed at potential scan rates typically in the 0.05-10 V/s range, using an Autolab 308 potentiostat (Metrohm Autolab) run by a PC with dedicated Nova 2.0 software. The samples were 0.5 mM solutions of each compound, deaerated by prolonged nitrogen bubbling, in a three-electrode conic cell (working volume 25 cm^3). The cell was equipped with a glassy carbon (GC) working electrode embedded in glass (Metrohm), a platinum counter electrode, and an aqueous saturated calomel electrode (SCE) as operating reference electrode. The latter was inserted in a compartment filled with the working solvent

with supporting electrolyte medium and communicating through a porous frit with the working electrode compartment, in order to avoid contamination of the latter by water and chloride leakage from the SCE. The working electrode potentials were normalized against the ferrocene/ferrocinium redox couple, recommended by IUPAC as intersolvental reference [23], by recording its CV pattern in the same experimental conditions as the investigated molecules, although in a separate experiment in order to avoid any possible interference. Compensation of the ohmic drop was performed by the positive feedback method. The cleanness of the working electrode surface was restored whenever necessary by mechanical treatment with artificial diamond powder (Aldrich, 1 μm diameter) on a wet cloth (STRUERS DP-NAP).

The reported CV patterns are the combination of a reduction half cycle obtained scanning the potential starting from 0 V vs SCE in the negative direction first, and of an oxidation half cycle, obtained scanning the potential from 0 V vs SCE in the positive direction first; this protocol ensures that the first oxidation and reduction take place on a clean surface, with no interference of the products of former ET processes.

HOMO and LUMO energy levels were calculated from the first oxidation and first reduction formal potentials (i.e. standard potentials neglecting activity coefficients, calculated as the average between forward and backward peak potential in the first oxidation and first reduction reversible peak systems respectively) by the following equations [24]:

$$E_{HOMO} \text{ (eV)} = -1 \text{ e} \times (E^{\circ\prime}I_{ox} \text{ vs } Fc^+|Fc \text{ /V} + 4.8 \text{ V } Fc^+|Fc \text{ vs } 0), \qquad (1)$$

$$E_{LUMO} \text{ (eV)} = -1 \text{ e} \times (E^{\circ\prime}I_{red} \text{ vs } Fc^+|Fc \text{ /V} + 4.8 \text{ V } Fc^+|Fc \text{ vs } 0). \qquad (2)$$

Absorption and emission spectra, both at RT and 77K, were measured in a 4 to 1 v/v ethanol - methanol mixture. UV/Vis absorption spectra were obtained on a Shimadzu UV-3600 Plus UV-VIS-NIR Spectrophotometer in 1 cm path length quartz cell. Photoluminescence quantum yields were measured with a C11347 Quantaurus - QY Absolute Photoluminescence Quantum Yield Spectrometer (Hamamatsu Photonics UK), equipped with a 150 W Xenon

lamp, an integrating sphere and a multi-channel detector. Steady state emission and excitation spectra and photoluminescence lifetimes were obtained with a FLS 980 spectrofluorimeter (Edinburg Instrument Ltd.). Continuous excitation for the steady state measurements was provided by a 450 W Xenon arc lamp. Emission spectra were corrected for the detector sensitivity and the reference excitation light recorded for stability control. Photoluminescence lifetime measurements, determined by TCSPC (time-correlated single-photon counting) method, were performed using an Edinburgh Picosecond Pulsed Diode Laser EPL-445 (Edinburg Instrument Ltd.), with central wavelength 445 nm and repetition rates of 20 μs or 50 μs, or a monochromated pulsed 150 W MicroFlash lamp. Photoluminescence and quantum yield (QY) experiments at room temperature were carried out in nitrogen degassed solution of the complexes 2×10^{-5} M. Acid-base titrations were conducted by adding small aliquot of trifluoroacetic acid (TFA) or trietylamine (TEA) in diluted solution of 4 to 1 v/v ethanol - methanol mixture (concentration ca 1×10^{-3} M). The diffuse reflectance UV-Visible spectra (DRUV-Vis) were recorded on a Jas.co V650 spectrometer (JASCO) equipped with 60 mm integrating sphere.

2.3. Photovoltaic performance

All chemicals used were of analytical grade and were used as received without any additional purification. The procedure used for preparation of the titania electrodes was similar to those described elsewhere [25, 26] and was as follows: 3 mL titanium tetraisopropoxide (Aldrich) were added to 13.5 mL of ethylene glycol (Aldrich) magnetically stirred at 333 K. The mixture, after addition 12.6 g of citric acid monohydrate (Aldrich), was heated under stirring at 363 K, until clear. The transparent sol obtained was mixed with 5.6 g P25 TiO_2 Aeroxide (Evonik) by grinding in agate mortar for 1 hour. The viscous titania paste obtained was spread on fluorine doped tin oxide (FTO) conductive glass substrate (Solaronix) using "doctor blade" technique

and sintered in air at 723 K for 1 hour. To prepare working electrodes for DSSCs, titania electrodes were immersed in 1×10^{-4} M solution of **RuLomp** dyes in absolute ethanol at ambient temperature in dark overnight. After dye adsorption, the electrodes were washed with absolute ethanol and dried in hot air stream. Platinum film coated FTO was used as a counter electrode. The typical cell was assembled using a 25 μm thick, hot-melted, ionomeric foil (Solaronix) as a sealant and a spacer between the electrodes and an electrolyte (a mixture of 0.6 M 1-propyl-3-methyl-imidazolium iodide (Aldrich), 0.03 M iodine (Aldrich), 0.1 M guanidine thiocyanate (Fluka) and 0.5 M 4-tert-butylpiridine (Aldrich) in acetonitrile (Merck)) were injected within two holes predrilled in the counter electrode. The final sealing was realized with the use of hot melted sealant and a microscope cover slide. The typical active area of the obtained DSSC was approximately 0.125 cm^2. Five cells representing each type were prepared and the results obtained for the best ones are presented. To determine the amount of dye adsorbed, the electrodes of the area 1.5 cm^2 were prepared and after dye adsorption they were immersed in 5 mL of NH$_4$OH solution (obtained by diluting of 1 mL of 25% NH$_4$OH (POCh) in water with 95% ethanol (Destylacje Polskie) to the volume of 10 mL) for 10 min. Concentration of the desorbed dye in the solution was determined by UV-Vis technique using Varian Cary 50 Probe spectrometer (Varian). For Raman scattering and reflectance spectroscopy measurements 5 μm thick TiO$_2$ films deposited onto microscope glass slide substrates were prepared by a screen printing technique using a paste prepared by the method described elsewhere [27] and the detailed procedure was as follows: 3 g of P25 TiO$_2$ Aeroxide (Evonik) were mixed with 0.5 mL of acetic acid (Aldrich) and 20 mL of ethanol (Aldrich) and kept in an ultrasonic bath for 3 h. A solution of 1.5 g ethyl cellulose (Aldrich) and 10 ml of α-terpineol in 13.5 g of ethanol was prepared in the meantime and then added to the former solution and the mixture was sonicated for additional hour. Afterwards, the mixture obtained was magnetically stirred overnight. Finally, ethanol was slowly removed on a rotary evaporator and the paste was ready-to-use.

Directly after calcination at 773K for 1 h the electrodes were kept at 353K. Afterwards, they were immersed in a 1×10^{-4} M ethanolic solutions of a **RuLomp** dyes at 313K for 1, 5, 10, 15, 30, 60, 90 and 120 min, and subsequently rinsed in ethanol to remove any unadsorbed dye molecules from the nanoporous TiO_2 films. Raman scattering spectroscopy measurements were carried out at room temperature using a confocal micro-Raman spectrometer (InVia, Renishaw) and a 514 nm argon ion laser, operating at a 10% of its total power (50 mW), as the excitation.

The photovoltaic characteristics (J-V curves) of the cells were measured using a Sun 2000 class A solar simulator (Abet Technologies) equipped with an AM 1.5G filter, with the light intensity adjusted at 100 mW·cm^{-2} using a silicon reference cell (ReRa Systems). J-V curves were recorded on a Keithley 2400 SourceMeter (Keithley). Incident photon to current conversion efficiency (IPCE) was measured by using Bentham PVE300 EQE/IPCE (Bentham) device and the measurement were made with the spectral resolution of 5 nm. Electrochemical impedance spectra (EIS) were recorded under standard AM 1.5G solar irradiation, obtained from Oriel 81172 class A solar simulator (Oriel), and V_{OC} forward bias conditions in the frequency range from 0.1 Hz to 100 kHz, with $V_{AC} = 100$ mV and recorded on Autolab 308 Potentiostat Galvanostat (Metrohm Autolab).

2.4. Theoretical calculations

Structures of the **RuLomp** dyes were initially optimized by semi-empirical calculations. The geometric optimization was carried out, as in our previous work [28], by parametric method 6 (PM6) using the Scigress 2.1.0 program [29]. Then, the total energy minimization procedures were carried out for all studied dyes using the density functional theory (DFT) applied in the GAUSSIAN 03 package [30]. The geometries were optimized according to Becke's three parameters hybrid method with the Lee, Yang and Parr correlation functional (B3LYP) [31-33] and 3-21G basis set for all remaining atoms. To model the TiO_2 nanoparticles and surfaces, we

considered $(TiO_2)_{76}$ clusters which were obtained by appropriately "cutting" the anatase slab exposing the (101) surface.

For better accuracy, in the next step, the geometry of all molecules was optimized applying the *ab initio* formalism implemented in GAMESS program package [34, 35]. The procedure was performed for isolated molecule in vacuum. The initial geometry was built up using the ACD/ChemSketch, an integrated software package from Advanced Chemistry Development, Inc. The minimum of the potential energy surface was calculated at restricted Hartree-Fock (RHF) level [36] for neural molecules with the 3-21G basis set applied for Ru atom and with the 6-311G basis set for all remaining atoms. The calculations were performed for molecules in C1 defined symmetry. The quadratic approximation (QA) optimisation algorithm [37] based on augmented Hessian techniques was used to reach the geometry of the investigated molecules characterized by a minimum of the total energy. The gradient convergence tolerance was equal to 10^{-4} Hartree/Bohr. At the end of the geometry optimization the Hessian evaluation was performed to exclude the structures giving negative modes and ensure the thermodynamic equilibrium of the molecule.

To predict electronic properties of the investigated molecules the quantum chemical calculations were performed using the structure with optimized geometry. The electronic properties were computed for the isolated molecules as well as for molecules dissolved in methanol/ethanol solvent. The calculations were carried out applying density functional theory (DFT) methodology using GAMESS program package [34, 35]. The time dependent DFT (TDDFT) formalism was considered to be the most prominent method to calculate the excited state of medium-size and large molecules. The TDDFT calculations were performed using different exchange-correlation (XC) potentials in generalized gradient approximation (GGA), namely the B3LYP [31-33], LC-BLYP [38] and CAM-B3LYP [39] potentials. The single point calculations were performed with the 3-21G basis set applied for Ru atom and with the 6-311G

basis set for all other atoms. The RHF SCF energy convergence criterion was chosen to be 10^{-12} Hartree. The UV-Vis absorption spectra were calculated using the iterative Davidson method [40] with an accuracy of 10^{-12} Hartree. In order to investigate the solvent effect on the electronic properties of **RuLomp** molecules, the Polarizable Continuum Model (PCM) [41] was used, applying the conductor-like PCM (C-PCM) [42, 43] implementation. It is one of the most frequently used apparent surface charge (ASC) model [44, 45]. The solvent radii and the dielectric constants were assumed to be the same as the parameters collected in GAMESS code. To model the TiO_2 nanoparticles and surfaces, the $(TiO_2)_{76}$ clusters obtained by appropriately "cutting" an anatase slab exposing the (101) surface were considered.

2.5. Other analytical methods

All NMR spectra were measured on an Agilent DD2 spectrometer (Agilent Technologies, USA), operating at frequencies 799.86 MHz for ^1H and 201.15 MHz for ^{13}C, equipped with 5 mm $^1H/^{13}C/^{15}N$ triple resonance probe. The sample temperature was stabilized at 298 K. Chemical shifts were referred to the signal of internal TMS (0.00 ppm). High-resolution mass spectra were recorded on an AMD 402 two-sector mass spectrometer (AMD Intectra, Germany) of B/E geometry using a peak matching technique. Elemental compositions of the ions discussed were determined with an error of less than 10 ppm in relation to perfluorokerosene at a resolving power of 10000. ESI Mass spectra were recorded on a Waters/Micromass Q-tof Premier (ESI-MS) mass spectrometer (Waters Ltd., Eltree, UK) using acetonitrile solutions of compounds studied (ca. 1×10^{-4} M). Elementary analyses were obtained on a Vario EL III (Elementar Analysensysteme GmbH, Hanau, Germany) analyser. Melting points were measured on Mel-Temp apparatus (Barnstead/Thermolyne Corp., USA).

3. Results and Discussion

3.1. Synthesis and characterization

3- and 4-substituted bipyridine ligands (***m*-4** and ***p*-4**) were synthesized by Sonogashira coupling of corresponding ethyl ethynylbenzoates with 4-bromo-2,2'-bipyridine and further deprotection of carboxyl group (Scheme 1). This route failed for *ortho* isomer, as the hydrolysis of ethyl ester ***o*-3** in basic conditions results in rearrangement and formation of 2-substituted 1,3-indanedione (see Supporting Information for details; Scheme S1). As the acidic hydrolysis of the above-mentioned ester does not occur, the ligand ***o*-4** was synthesized by coupling of 4-ethynyl-2,2'-bipyridine with *O*-trimethylsilyl protected 2-bromobenzoic acid (Scheme 2). The second substrate was synthesized by the method of Bruynes and Jurriens [46]. The complexes studied were synthesized from bis(2,2'-bipyridine)ruthenium(II) dichloride and corresponding ligands by standard procedure and purified by precipitation in form of hexafluorophosphate salts (Scheme 3). All compounds were obtained in good yield and purity. Their NMR spectra are presented in Supporting Information.

3.2. Electrochemical and photophysical properties

The electrochemical characteristics of **RuLomp** dyes as well as three literature and/or commercial reference ruthenium complexes (Ru(bpy)$_3$$^{2+}$, 455PF6 and B1 dyes) were obtained by cyclic voltammetry and the relevant cyclic voltammograms (the *j-E* curves) are presented in Figure 1, while the electrochemical parameters are collected in Table 1. To support the main findings, the electrochemical characterization of the free ligands has been also investigated and the full discussion is presented in Supporting Information. The monoelectronic oxidation peak, corresponding to $Ru^{2+} \rightarrow Ru^{3+} + e^-$ process, reversible both chemically and electrochemically can be observed on *j-E* curves recorded for all investigated complexes (the additional oxidation signal on Ru(bpy)$_3$$^{2+}$, which was in chloride salt form, CV pattern recorded at about 0.62 V

corresponds to the Cl⁻ ions [47]). The potentials of the oxidation peaks, observed for the **RuLomp** complexes, are slightly more positive, with respect to those for Ru(bpy)$^{2+}$ reference and this effect is a consequence of the presence of the electron attracting, anchoring COOH groups in the **Lomp** ligands. The strongest effect is observed on the 455PF6 CV pattern, because this molecule has two COOH groups located on one bipyridine ligand. Therefore, also the HOMO levels of **RuLomp** dyes are slightly lowered when compared with that of Ru(bpy)$_3^{2+}$ complex. The reduction part of the CV curves is much more complex than the oxidation one. All the complexes investigated undergo a multistep reduction process. Moreover, the CV curves of the dyes with COOH anchoring groups show a very interesting sharp signal associated with adsorptive phenomena or sudden charge releases connected with structural rearrangements or unstable radical formation and this process will be the goal of our further investigation. Here we focus on the first reduction process which most probably occurs on the **Lomp** ligands. When compared to the free ligands (see Supporting Information) the first reduction peaks of the complexes are much more positive (-1.69 V vs -2.32 V with **Lm**, -1.66 V vs -2.17 V with **Lp**, -1.67 V vs -2.17 V with L1) and this effect can be explained by the donation of electrons to the central metal so that the ligands become electron-poorer. The complexation makes the ligands (the radical ions) more stable, which may be deduced from the higher chemical reversibility of the first reduction peak. Furthermore, the electrochemical reversibility is still high (fast reduction processes). In **RuLo** the first reduction process potential is significantly more positive than in the *meta* and *para* ones (easier reduction), but the stability of the electron transfer product is lower (nearly no return peak, and dEp/d*log*v slope of about 40 mV consistent with the electron transfer step followed by a chemical one). *Ortho* substitutes very often show very peculiar behavior (for instance the Hammet constant [48] are mostly given only for *para* and *meta* substitutes; the **RuLo** dye synthesis is also much more difficult and cannot be carried out by standard methods as for the other two presented dyes). The increased conjugated system of

the double bonds together with the conjugated electron attracting COOH groups in the dyes studied, results that the first reduction signals are shifted to more positive values than in the Ru(bpy)$_3^{2+}$ (-1.49 – -1.69 V vs -1.76 V, respectively). Moreover, the 455PF6 dye, including a bipyridyl ligand bearing two carboxylic groups, has the first reduction process even more positive (peak at -1.19 V) which may support the explanation of the COOH group influence on the **RuLomp** properties. Such behavior, however, indicates a significantly lower LUMO level of **RuLomp** dyes. Therefore, also the HOMO energy level should be lower, but to a smaller degree than the LUMO one; thus, the energy gap for our dyes is narrower than that of Ru(bpy)$_3^{2+}$ reference one, besides being shifted to lower energy values (see Table 1).

The UV/Vis/NIR absorption spectra of the three complexes, in the MeOH-EtOH mixture, recorded at 298 K are reported in Figure 2a. The three spectra are quite similar to one other with only a few differences. The three complexes display 3 major absorption bands at 245, 290, 330 nm and a broader one, in the visible region, between 400-520 nm. Ru(II) bipyridyl derivatives have been widely studied earlier. Taking in the account the early work of Balzani et.al. [49] the absorption bands below 220 nm and at 290 nm can be ascribed to π-π* electron transition in the ligands, while the 245 nm band and the one in the visible range are assigned to metal to ligand charge transfer (MLCT) transitions. The absorption spectra in the visible range have a quite long tail spreading up to 600 nm. These tails become more resolved in the 77 K excitation measurements (see Supporting Information Figure S17) assuming the shape of a shoulder around 550 nm. Their relatively low molar absorptivity suggests that these absorption features can be assigned to the transition involving [3]MLCT states.

Comparing the three spectra, two specific features can be noted. The UV spectra of **RuLp** and **RuLm** systems are almost identical, in the spectrum of **RuLo** complex, the low energy band (476 nm vs. 460 nm, see table 2) is shifted by about 16 nm to the red and shows slightly larger molar absorptivity at 250 nm. The second interesting feature concerns to the band

that appears around 330 nm in the **RuLo** and **RuLm** complexes (whereas the same band appears, as a shoulder, under the 290 nm main band). This band, at least in the spectra of **RuLm** and **RuLp**, strongly responds to changes in pH such as it is located at shorter wavelength in acidic conditions and is red-shifted, upon deprotonation. On average, we observe a bathochromic shift, in basic media, by about 7 nm (see Supporting Information Figure S18). Therefore, this band can be ascribed to transitions involving the ligand (carrying the carboxylate group) responsible for the anchoring onto the TiO_2 surface. This observation may suggest that **RuLm** and **RuLp** are probably deprotonated in the methanol-ethanol solution, which can increase their adsorption abilities on the titania surface. On the other hand, the carboxylic anchor of **RuLo** may be involved in some strong intramolecular interactions (no pH dependence) and it may have strong negative impact on the chemisorption abilities of the **RuLo** dye on the titania surface [50] (see further discussion).

The photophysical properties of the complexes have been analyzed in terms of photoluminescence quantum efficiency and lifetimes, both at room temperature, in diluted solution, and at 77 K, in a rigid matrix. The three complexes show broad featureless emission, at room temperature, between 550-850 nm with full width half maximum (FWHM) of about 2600 cm^{-1} and overall lifetime in the microsecond range (Figure 2b and Table 2). The strong intersystem crossing (ISC) in Ru complexes together with the large Stokes shift observed between the absorption and emission spectra (175-195 nm) allow assignment the emission to the ^{3}MLCT state. The emission peak maxima are located at 635 nm for **RuLp** and 633 nm for **RuLm** whereas in the emission spectrum of complex **RuLo** has a maximum shifted to 670 nm mirroring the corresponding shift of the absorption spectrum. The two derivatives, **RuLp** and **RuLm,** display very similar photophysical behavior while the major differences can be again observed in the *ortho* derivative. In particular, their luminescence quantum efficiency of ca. 0.18-0.19 is almost twice as large as that of the **RuLo** derivative (0.095).

Interestingly, the PL lifetime is similar for all the complexes; 1.97, 1.89 and 1.90 μs for **RuLp**, **RuLm** and **RuLo** respectively. This implies that the radiative rate constant (k_r) of **RuLp** and **RuLm** are doubled in comparison to that of **RuLo**, while the nonradiative (k_{nr}) rate components are of the same magnitude for the three complexes. The nonradiative rate constant k_{nr} seems to be independent of the position of the carboxylic functional group. This trend is interesting since does not follow the behavior expected if the rate constants simply obey the energy gap law [51, 52]. Accordingly, the nonradiative decay rate constants for **RuLo** complex with the lowest energy HOMO-LUMO gap would be expected to surpass those of the **RuLp** and **RuLm** complexes.

At 77 K (Figure 2c) the phosphorescence emissions undergo a typical rigidochromic blue-shift of about 24 – 20 nm and they become vibrationally resolved with progression spacing in the range of 1100-1400 cm^{-1}. The PL lifetimes measured at low temperature (7.0, 6.44 and 6.28 μs for **RuLp**, **RuLm** and **RuLo**, respectively) are ca. 3-3.5 times longer than those at room temperature. Assuming a unitary Φ_{ISC}, the above observation implies that while in the complexes **RuLp** and **RuLm** the non-radiative decays roughly become one order of magnitude smaller compared to that of RT, in **RuLo** k_{nr} the nonradiative decay is reduced only by one fifth. Therefore, in these conditions the expected increase in the nonradiative rate constants of **RuLo**, as a consequence of the emission red-shift takes place. This reasoning assumes that the average radiative rate constant (k_r) for zero-field split (ZFS) triplet manifold weakly depend on temperature in the respective temperature range, similarly as observed for Ir(ppy)$_3$ complex with higher triplet sublevels energy splitting (83 cm^{-1} in comparison to 60 cm^{-1} for Ru(bpy)$_3^{2+}$) [53].

As already mentioned, before starting the essential calculations the geometries of the **RuLomp** molecules were optimized using the HF/3-21G(Ru)6-311G methodology. Also, the DFT methodology was used to optimize studied structures but the obtained results were

unsatisfactory. It is known that the DFT/GGA and hybrid functional tend to overestimate the interatomic distances [54, 55]

The chemical structures of all studied molecules after geometry optimization procedure are presented in Figure S22. The structures of investigated molecules differ by the carbon chain connecting Ru complex and phenyl group. The torsional angle created by carbon chain is equal 6.84° and 5.70° for **RuLm** and **RuLp** molecules, respectively and 31.15° for **RuLo** molecule. The phenyl group is twisted in relative to Ru complex plane. The twisting angle is equal to 65.43° and 66.70° for **RuLm** and **RuLp** molecules, respectively and 60.04° for **RuLo** molecule. The carboxylic group is distant from phenyl group by 1.48 Å for **RuLm** and **RuLo** molecules and by 1.36 Å for **RuLp** molecule. From the structural point of view the **RuLm** and **RuLp** molecules are more planar when compared to the **RuLo** molecule.

The electronic properties of all investigated molecules were calculated applying the DFT methodology with different functionals, namely B3LYP, LC-BLYP and CAM-B3LYP with 3-21G basis set for Ru atom and 6-311G basis set for all remaining atoms. The results in the best agreement with the experimental UV-vis absorption spectra, were obtained by DFT/LC-BLYP methodology (see Figure S23). The electronic properties of studied molecules are given in Table S3. The carboxylic group in *para* position increases the value of the electric dipole moment (μ) of the molecule but the lowest dipole moment is obtained for the **RuLo** molecules. The decrease in the dipole moment in the direction from **RuLp**, through **RuLm** to **RuLo** may strongly influence the decrease in the photovoltaic performance, especially the photovoltage (V_{OC}) values, changing in the same direction [56, 57]. Also, the changes in electronegativity (χ) and chemical hardness (η), which affect the chemical reactivity and photovoltaic properties of the dyes [58], show the same tendency as the dipole moment of the molecules. These results are in good agreement with the above-mentioned observations that the stability of the electron occurring as product of the electrochemical reduction process in the

RuLo complex is lower than in the other two dyes. It can be ascribed to significantly lower electronegativity and chemical hardness of the *ortho* moiety than those of the *para* and *meta* ones. The same tendency can be also observed for $\Delta E_{HOMO-LUMO}$ values, which is also in a good agreement with our electrochemical studies. However, the calculated values quantitatively do not correspond with the experimental data as far as the HOMO and LUMO levels are concerned. The calculated values are not sufficient for the dyes to be applied in DSSC's which requires that the LUMO level of the dye must be higher than the titania conduction band level (about -4.0 eV) and the HOMO level should be more negative than the redox potential of the electrolyte (about -4.8 eV for iodine electrolytes) [59] however this disagreement is a computational error related to the methodology used for quantum chemical calculations.

3.3. Photovoltaic performance

Figure 3 shows the incident photon to current efficiencies (IPCE) spectra, plotted as a function of excitation wavelength, for the photovoltaic devices sensitized by **RuLomp** dyes. The photocurrent action spectra well correspond to the visible region absorption spectra of the investigated sensitizers and the maximum IPCE values, i.e. 2.23, 4.89 and 6.96 % for **RuLo**, **RuLm** and **RuLp** dyes, respectively, were obtained at the wavelengths which correspond with the MLCT bands of the dyes.

Photovoltaic performance of the DSSC devices sensitized by **RuLomp** dyes was tested under simulated solar irradiation and the results are collected in Table 3 while the photovoltage-photocurrent density curves are presented in Figure 4. The general observation is that the overall photon-to-current efficiency (η) of **RuLp** dye sensitized device is the best one, **RuLm** is the second best with about twice lower efficiency than **RuLp** and **RuLo** is the worst with again about twice lower efficiency than **RuLm**. The η values are in good agreement with the IPCE results. While there are no spectacular differences in open-circuit photovoltage (V_{OC}) values which are 534, 518 and 560 mV for **RuLo**, **RuLm** and **RuLp**, respectively, the photocurrent

densities (J_{SC}) differ significantly and the tendency is similar to that of the overall efficiency values. It is well known that the J_{SC} strongly depends on electron injection, recombination and transportation through the semiconducting electrode process as well as on the number of dye molecules adsorbed on the semiconductor surfaces [3, 60-62]. The electron transportation process is less important in our investigation, because the titania electrodes used for DSSCs assembling were exactly of the same type for all the devices in this study and should not have a significant influence on the cells performances. The dye loading parameter (see the N_{dye} values in Table 3) determined for all the cells investigated show a significantly lower concentration of the **RuLo** adsorbed on the titania electrode surface, when compared to those of the other two dyes. Such a poor adsorption of the **RuLo** is most probably a consequence of the steric hindrance between the bulky ruthenium complex moiety and the titania surface, which has adverse effect on the chemical reaction between anchoring carboxylic group and surface hydroxyl groups, thus weaking the adsorption abilities of the **RuLo**. The N_{dye} value determined for the **RuLm** is also a little bit lower when compared with that of **RuLp** and can be one of the reasons for the poorer efficiency of the **RuLm** sensitized cells. Direct observation of the dyes adsorption dynamics studied by Raman spectroscopy [63] (see Figure S20a-c in Supporting Information) shows that the saturation of the adsorption process for all the three dyes presented is reached after 90 min. of the sample dipping in the dye solution at 40˚C. However, the degree of the electrode surface coverage, examined by diffuse reflectance UV-Vis technique for the dyes is good agreement with the N_{dye} values (see Figure S21). According to our quantum-mechanical calculations the low amount of the **RuLo** dye is mostly due to the unsuitable geometry of the molecule, which leads to the energetically unfavorable adsorption process (see Scheme 4 and Table S2). Additionally, we observed that although **RuLo** dye is adsorbed efficiently, it can be easily washed off with acetonitrile and finally only a small amount of the initially adsorbed dye remains on the surface. This observation suggests that the physisorption

occurs more efficiently than chemisorption in the **RuLo** dye case. This effect may be also enhanced, in addition to the steric hindrance, by the specific electronic properties of **RuLo** as observed in our photophysical studies. Accordingly, the anchoring group being involved in the strong intramolecular interaction with bipyridine Ru complex unit, loses partly its ability to bond the semiconductor surface.

To better understand the electron injection and recombination processes taking place in the investigated cells, the electrochemical impedance spectroscopy (EIS) measurements were performed, as this technique is well known to be useful in investigation of these processes [18, 64]. Figure 5 presents the Nyquist plots of impedance spectra of the cells sensitized with the **RuLomp** dyes, also an electrical equivalent circuit used for the experimental data fitting and the values for each parameter obtained are collected in Table 4. The ohmic serial resistance, R_1, observed at the high frequencies represents the FTO resistance and the values found are similar for all three types of the cells. The resistance of the redox charge transfer process at the Pt electrode of the solar cell values, R_2, observed at the high-frequencies, are more varied and it could be caused by the differences in the Pt film thickness and/or existence of discontinuities in the Pt layer on the counter electrode [65, 66]. The R_3 values, which correspond to the electron transfer process at the TiO_2/dye/electrolyte interface, recorded for **RuLomp** dyes are 1237.0, 1076.0 and 356.2 Ω for **RuLo**, **RuLm** and **RuLp**, respectively. Clearly higher R_3 values in **RuLo** and **RuLm** sensitized solar cells indicate an increase in the electron recombination resistance and poorer electron injection efficiency when compared to those of the **RuLp** sensitized cell and these phenomena may explain the lower efficiencies of the two former cells [67]. Moreover, the highest R_3 value recorded for **RuLo** cell can be, in combination with the low N_{dye} value, the reason for very low efficiency of such cells. On the other hand, in the **RuLm** sensitized cell, the high N_{dye} value (the larger amount of adsorbed dye molecules) partly eliminates the negative influence of recombination process, which improves the cell efficiency.

The EIS results are in good agreement with our voltammetry and spectroscopic studies as well as quantum-mechanical calculations and reveal that the *para*-located anchoring group has the strongest influence on electron injection process, which in combination with the good dye adsorption on the titania electrode surface leads to the best performance of the solar cells sensitized with this compound.

4. Conclusions

Concluding, in this article we have shown that the position of a single anchoring group in the dye molecule has significant influence on the performance of DSSCs. The number of chemisorbed dye molecules is the main factor limiting the cell efficiency. It can be observed that in the cells sensitized with ortho-substituted dye the steric hindrance in combination with specific intramolecular interactions suppressed the dye adsorption ability, and in this way worsened the performance parameters of the devices. On the other hand, the resonance structures of benzene ring in anchoring ligand have high impact on the electron transfer process at the TiO_2/dye/electrolyte interface which is quantified by R_3 resistance value affecting significantly the cells efficiency. For meta and para-moieties, the number of adsorbed dyes molecules were similar, but the R_3 values differed significantly which resulted in better performance (with two times higher η value) of the cells sensitized with the latter dye. In opposite to the earlier published papers describing ruthenium dyes with two or more anchoring groups, for which the most important factor determining efficiency of the cell was the geometry and steric hindrance of the molecules during the adsorption on the electrode surface, here we clearly show that intramolecular electron transfer and electron injection abilities depend also on the anchoring group position. Our findings are of importance for further development of new sensitizers that would deliver the highest possible photoconversion efficiency of DSSCs.

5. Acknowledgments

6. References

[1] M. Gratzel, Photoelectrochemical cells, Nature, 414 (2001) 338-344.
[2] M. Grätzel, Dye-sensitized solar cells, Journal of Photochemistry and Photobiology C: Photochemistry Reviews, 4 (2003) 145-153.
[3] A. Hagfeldt, G. Boschloo, L. Sun, L. Kloo, H. Pettersson, Dye-Sensitized Solar Cells, Chem. Rev., 110 (2010) 6595-6663.
[4] A. Hagfeldt, M. Grätzel, Molecular Photovoltaics, Acc. Chem. Res., 33 (2000) 269-277.
[5] G.C. Vougioukalakis, A.I. Philippopoulos, T. Stergiopoulos, P. Falaras, Contributions to the development of ruthenium-based sensitizers for dye-sensitized solar cells, Coord. Chem. Rev., 255 (2011) 2602-2621.
[6] M. Grätzel, Recent Advances in Sensitized Mesoscopic Solar Cells, Acc. Chem. Res., 42 (2009) 1788-1798.
[7] S. Mathew, A. Yella, P. Gao, R. Humphry-Baker, B.F.E. Curchod, N. Ashari-Astani, I. Tavernelli, U. Rothlisberger, M.K. Nazeeruddin, M. Grätzel, Dye-sensitized solar cells with 13% efficiency achieved through the molecular engineering of porphyrin sensitizers, Nature Chemistry, 6 (2014) 242-247.
[8] T. Higashino, H. Imahori, Porphyrins as excellent dyes for dye-sensitized solar cells: recent developments and insights, Dalton Transactions, 44 (2015) 448-463.
[9] M. Ishida, D. Hwang, Z. Zhang, Y.J. Choi, J. Oh, V.M. Lynch, D.Y. Kim, J.L. Sessler, D. Kim, β-Functionalized Push–Pull Porphyrin Sensitizers in Dye-Sensitized Solar Cells: Effect of π-Conjugated Spacers, ChemSusChem, 8 (2015) 2967-2977.
[10] C.-W. Lee, H.-P. Lu, C.-M. Lan, Y.-L. Huang, Y.-R. Liang, W.-N. Yen, Y.-C. Liu, Y.-S. Lin, E.W.-G. Diau, C.-Y. Yeh, Novel Zinc Porphyrin Sensitizers for Dye-Sensitized Solar Cells: Synthesis and Spectral, Electrochemical, and Photovoltaic Properties, Chemistry – A European Journal, 15 (2009) 1403-1412.
[11] T. Funaki, M. Yanagida, N. Onozawa-Komatsuzaki, Y. Kawanishi, K. Kasuga, H. Sugihara, Ruthenium (II) complexes with π expanded ligand having phenylene–ethynylene moiety as sensitizers for dye-sensitized solar cells, Solar Energy Materials and Solar Cells, 93 (2009) 729-732.
[12] K.L. Vincent Joseph, A. Anthonysamy, R. Easwaramoorthi, D.V. Shinde, V. Ganapathy, S. Karthikeyan, J. Lee, T. Park, S.-W. Rhee, K.S. Kim, J.K. Kim, Cyanoacetic acid tethered thiophene for well-matched LUMO level in Ru(II)-terpyridine dye sensitized solar cells, Dyes and Pigments, 126 (2016) 270-278.

[13] M. Zalas, B. Gierczyk, M. Klein, K. Siuzdak, T. Pędziński, T. Łuczak, Synthesis of a novel dinuclear ruthenium polypyridine dye for dye-sensitized solar cells application, Polyhedron, 67 (2014) 381-387.

[14] M. Zalas, B. Gierczyk, M. Cegłowski, G. Schroeder, Synthesis of new dendritic antenna-like polypyridine ligands, Chem. Pap., 66 (2012) 733-740.

[15] T.J. Meyer, G.J. Meyer, B.W. Pfennig, J.R. Schoonover, C.J. Timpson, J.F. Wall, C. Kobusch, X. Chen, B.M. Peek, Molecular-Level Electron Transfer and Excited State Assemblies on Surfaces of Metal Oxides and Glass, Inorg. Chem., 33 (1994) 3952-3964.

[16] Y.-j. Hou, P.-h. Xie, B.-w. Zhang, Y. Cao, X.-r. Xiao, W.-b. Wang, Influence of the Attaching Group and Substituted Position in the Photosensitization Behavior of Ruthenium Polypyridyl Complexes, Inorg. Chem., 38 (1999) 6320-6322.

[17] R. Argazzi, N.Y. Murakami Iha, H. Zabri, F. Odobel, C.A. Bignozzi, Design of molecular dyes for application in photoelectrochemical and electrochromic devices based on nanocrystalline metal oxide semiconductors, Coord. Chem. Rev., 248 (2004) 1299-1316.

[18] A.S. Hart, C.B. Kc, H.B. Gobeze, L.R. Sequeira, F. D'Souza, Porphyrin-Sensitized Solar Cells: Effect of Carboxyl Anchor Group Orientation on the Cell Performance, ACS Applied Materials & Interfaces, 5 (2013) 5314-5323.

[19] J. Chen, Y. Sheng, S. Ko, L. Liu, H. Han, X. Li, Push-pull porphyrins with different anchoring group orientations for fully printable monolithic dye-sensitized solar cells with mesoscopic carbon counter electrodes, New J. Chem., 39 (2015) 5231-5239.

[20] R.B. Ambre, S.B. Mane, G.-F. Chang, C.-H. Hung, Effects of Number and Position of Meta and Para Carboxyphenyl Groups of Zinc Porphyrins in Dye-Sensitized Solar Cells: Structure–Performance Relationship, ACS Applied Materials & Interfaces, 7 (2015) 1879-1891.

[21] K. Kilså, E.I. Mayo, D. Kuciauskas, R. Villahermosa, N.S. Lewis, J.R. Winkler, H.B. Gray, Effects of Bridging Ligands on the Current−Potential Behavior and Interfacial Kinetics of Ruthenium-Sensitized Nanocrystalline TiO2 Photoelectrodes, The Journal of Physical Chemistry A, 107 (2003) 3379-3383.

[22] V. Grosshenny, F.M. Romero, R. Ziessel, Construction of Preorganized Polytopic Ligands via Palladium-Promoted Cross-Coupling Reactions, The Journal of Organic Chemistry, 62 (1997) 1491-1500.

[23] G. Gritzner, J. Kuta, International union of pure and applied chemistry physical chemistry division commission on electrochemistry recommendations on reporting electrode potentials in nonaqueous solvents, Pure and Applied Chemistry, 56 (1984) 461-466.

[24] C. Baldoli, S. Bertuolo, E. Licandro, L. Viglianti, P. Mussini, G. Marotta, P. Salvatori, F. De Angelis, P. Manca, N. Manfredi, A. Abbotto, Benzodithiophene based organic dyes for DSSC: Effect of alkyl chain substitution on dye efficiency, Dyes and Pigments, 121 (2015) 351-362.

[25] U. Opara Krasovec, M. Berginc, M. Hocevar, M. Topic, Unique TiO2 paste for high efficiency dye-sensitized solar cells, Solar Energy Materials and Solar Cells, 93 (2009) 379-381.

[26] M. Zalas, M. Walkowiak, G. Schroeder, Increase in efficiency of dye-sensitized solar cells by porous TiO2 layer modification with gadolinium-containing thin layer, Journal of Rare Earths, 29 (2011) 783-786.

[27] J. Sobuś, J. Kubicki, G. Burdziński, M. Ziółek, Carbazole Dye-Sensitized Solar Cells Studied from Femtoseconds to Seconds—Effect of Additives in Cobalt- and Iodide-Based Electrolytes, ChemSusChem, 8 (2015) 3118-3128.

[28] M. Klein, R. Pankiewicz, M. Zalas, W. Stampor, Magnetic field effects in dye-sensitized solar cells controlled by different cell architecture, Scientific Reports, 6 (2016) 30077.

[29] MO-G Version 1.1, in, Fujitsu Limited, Tokyo, Japan, 2008.

[30] M.J. Frish, G.W. Trucks, H.B. Schlegel, G.E. Scuseria, M.A. Robb, J.R. Cheeseman, J.A. Montgomery, T.K. Vreven, K. N., J.C. Burant, J.M. Millam, S.S. Iyengar, J. Tomasi, V. Barone, B. Mennucci, M. Cossi, G. Scalmani, N. Rega, G.A. Peterson, H. Nakatsuji, M. Hada, M. Ehara, K. Toyota, R. Fukuda, J. Hasegawa, M. Ishida, T. Nakajama, Y. Honda, O. Kiato, H. Nakai, M. Klene, X. Li, J.E. Knox, H.P. Hratchin, J.B. Cross, C. Adamo, J. Jaramillo, R. Gomperts, R.E. Startmann, O. Yazyev, A.J. Austin, R. Cammi, C. Pomelli, J.W. Octerski, P.Y. Ayala, K. Morokuma, G.A. Voth, P. Salvador, J.J. Dannenbeg, V.G. Zakrzewski, S. Dapprich, A.D. Daniels, M.C. Strain, O. Farks, D.K. Malick, A.D. Rabuck, K. Raghavachari, J.B. Foresman, J.V. Ortiz, Q. Cui, A.G. Baboul, S. Clifford, J. Cioslowski, B.B. Stefanov, G. Liu, A. Liashenko, P. Piskorz, I. Komaromi, R.L. Martin, D.J. Fox, T. Keith, M.A. Al-Laham, C.Y. Peng, A. Nanayakkara, M. Challacombe, P.M.W. Gill, B. Johnson, W. Chen, M.W. Wong, C. Gonzalez, J.A. Pople, Gaussian03, Revision B.04, in, Gaussian, Inc., Pittsburgh, PA, 2003.

[31] A.D. Becke, Density-functional exchange-energy approximation with correct asymptotic behavior, Physical Review A, 38 (1988) 3098-3100.

[32] A.D. Becke, Density- functional thermochemistry. III. The role of exact exchange, The Journal of Chemical Physics, 98 (1993) 5648-5652.

[33] C. Lee, W. Yang, R.G. Parr, Development of the Colle-Salvetti correlation-energy formula into a functional of the electron density, Physical Review B, 37 (1988) 785-789.

[34] M.W. Schmidt, K.K. Baldridge, J.A. Boatz, S.T. Elbert, M.S. Gordon, J.H. Jensen, S. Koseki, N. Matsunaga, K.A. Nguyen, S. Su, T.L. Windus, M. Dupuis, J.A. Montgomery, General atomic and molecular electronic structure system, J. Comput. Chem., 14 (1993) 1347-1363.

[35] M.S. Gordon, M.W. Schmidt, Chapter 41 - Advances in electronic structure theory: GAMESS a decade later A2 - Dykstra, Clifford E, in: G. Frenking, K.S. Kim, G.E. Scuseria (Eds.) Theory and Applications of Computational Chemistry, Elsevier, Amsterdam, 2005, pp. 1167-1189.

[36] C.C.J. Roothaan, New Developments in Molecular Orbital Theory, Reviews of Modern Physics, 23 (1951) 69-89.

[37] F. Jensen, Locating transition structures by mode following: A comparison of six methods on the Ar8 Lennard- Jones potential, The Journal of Chemical Physics, 102 (1995) 6706-6718.

[38] H. Iikura, T. Tsuneda, T. Yanai, K. Hirao, A long-range correction scheme for generalized-gradient-approximation exchange functionals, The Journal of Chemical Physics, 115 (2001) 3540-3544.

[39] T. Yanai, D.P. Tew, N.C. Handy, A new hybrid exchange–correlation functional using the Coulomb-attenuating method (CAM-B3LYP), Chem. Phys. Lett., 393 (2004) 51-57.

[40] E.R. Davidson, The iterative calculation of a few of the lowest eigenvalues and corresponding eigenvectors of large real-symmetric matrices, Journal of Computational Physics, 17 (1975) 87-94.

[41] S. Miertuš, E. Scrocco, J. Tomasi, Electrostatic interaction of a solute with a continuum. A direct utilizaion of AB initio molecular potentials for the prevision of solvent effects, Chem. Phys., 55 (1981) 117-129.

[42] V. Barone, M. Cossi, Quantum Calculation of Molecular Energies and Energy Gradients in Solution by a Conductor Solvent Model, The Journal of Physical Chemistry A, 102 (1998) 1995-2001.

[43] M. Cossi, N. Rega, G. Scalmani, V. Barone, Energies, structures, and electronic properties of molecules in solution with the C-PCM solvation model, J. Comput. Chem., 24 (2003) 669-681.

[44] J. Tomasi, B. Mennucci, R. Cammi, Quantum Mechanical Continuum Solvation Models, Chem. Rev., 105 (2005) 2999-3094.

[45] M. Cossi, B. Mennucci, R. Cammi, Analytical first derivatives of molecular surfaces with respect to nuclear coordinates, J. Comput. Chem., 17 (1996) 57-73.

[46] C.A. Bruynes, T.K. Jurriens, Catalysts for silylations with 1,1,1,3,3,3-hexamethyldisilazane, The Journal of Organic Chemistry, 47 (1982) 3966-3969.

[47] Y. Ohsawa, K.W. Hanck, M.K. DeArmond, A systematic electrochemical and spectroscopic study of mixed-ligand ruthenium(II) 2,2′-bipyridine complexes [Ru(bpy)3-nLn]2+ (n=0,1,2 and 3), Journal of electroanalytical chemistry and interfacial electrochemistry, 175 (1984) 229-240.

[48] C. Hansch, A. Leo, R.W. Taft, A survey of Hammett substituent constants and resonance and field parameters, Chem. Rev., 91 (1991) 165-195.

[49] A. Juris, V. Balzani, F. Barigelletti, S. Campagna, P. Belser, A. von Zelewsky, Ru(II) polypyridine complexes: photophysics, photochemistry, eletrochemistry, and chemiluminescence, Coord. Chem. Rev., 84 (1988) 85-277.

[50] M.K. Nazeeruddin, S.M. Zakeeruddin, R. Humphry-Baker, M. Jirousek, P. Liska, N. Vlachopoulos, V. Shklover, C.-H. Fischer, M. Grätzel, Acid−Base Equilibria of (2,2'-Bipyridyl-4,4'-dicarboxylic acid)ruthenium(II) Complexes and the Effect of Protonation on Charge-Transfer Sensitization of Nanocrystalline Titania, Inorg. Chem., 38 (1999) 6298-6305.

[51] J.V. Caspar, T.J. Meyer, Application of the energy gap law to nonradiative, excited-state decay, The Journal of Physical Chemistry, 87 (1983) 952-957.

[52] R. Englman, J. Jortner, The energy gap law for radiationless transitions in large molecules, Mol. Phys., 18 (1970) 145-164.

[53] W.J. Finkenzeller, H. Yersin, Emission of Ir(ppy)3. Temperature dependence, decay dynamics, and magnetic field properties, Chem. Phys. Lett., 377 (2003) 299-305.

[54] P.R. Carlier, N. Deora, T.D. Crawford, Protonated 2-Methyl-1,2-epoxypropane: A Challenging Problem for Density Functional Theory, The Journal of Organic Chemistry, 71 (2006) 1592-1597.

[55] K.P. Jensen, B.O. Roos, U. Ryde, Performance of density functionals for first row transition metal systems, The Journal of Chemical Physics, 126 (2007) 014103.

[56] P. Yu, F. Zhang, M. Li, R. He, Influence of position of auxiliary acceptor in D−A−π−A photosensitizes on photovoltaic performances of dye-sensitized solar cells, Journal of Materials Science, 50 (2015) 7333-7342.

[57] M.-W. Lee, J.-Y. Kim, H.J. Son, J.Y. Kim, B. Kim, H. Kim, D.-K. Lee, K. Kim, D.-H. Lee, M.J. Ko, Tailoring of Energy Levels in D-π-A Organic Dyes via Fluorination of Acceptor Units for Efficient Dye-Sensitized Solar Cells, Scientific Reports, 5 (2015) 7711.

[58] F. De Angelis, S. Fantacci, A. Sgamellotti, An integrated computational tool for the study of the optical properties of nanoscale devices: application to solar cells and molecular wires, Theor. Chem. Acc., 117 (2007) 1093-1104.

[59] J. Baldenebro-López, J. Castorena-González, N. Flores-Holguín, J. Almaral-Sánchez, D. Glossman-Mitnik, Computational Molecular Nanoscience Study of the Properties of Copper Complexes for Dye-Sensitized Solar Cells, International Journal of Molecular Sciences, 13 (2012) 16005-16019.

[60] B. Tripathi, P. Yadav, M. Kumar, Theoretical upper limit of short-circuit current density of TiO2 nanorod based dye-sensitized solar cell, Results in Physics, 3 (2013) 182-186.

[61] F.M. Rajab, Effect of Solvent, Dye-Loading Time, and Dye Choice on the Performance of Dye-Sensitized Solar Cells, Journal of Nanomaterials, 2016 (2016) 8.

[62] M. Zalas, M. Klein, The Influence of Titania Electrode Modification with Lanthanide Ions Containing Thin Layer on the Performance of Dye-Sensitized Solar Cells, International Journal of Photoenergy, 2012 (2012) 8.

[63] K. Suto, A. Konno, Y. Kawata, S. Tasaka, A. Sugita, Adsorption dynamics of the N719 dye on nanoporous titanium oxides studied by resonance Raman scattering and Fourier transform infrared spectroscopy, Chem. Phys. Lett., 536 (2012) 45-49.

[64] R. Cisneros, M. Beley, J.-F. Fauvarque, F. Lapicque, Investigation of electron transfer processes involved in DSSC's by wavelength dependent electrochemical impedance spectroscopy (λ-EIS), Electrochim. Acta, 171 (2015) 49-58.

[65] S. Cai, X. Hu, J. Han, Z. Zhang, X. Li, C. Wang, J. Su, Efficient organic dyes containing dibenzo heterocycles as conjugated linker part for dye-sensitized solar cells, Tetrahedron, 69 (2013) 1970-1977.

[66] M. Adachi, M. Sakamoto, J. Jiu, Y. Ogata, S. Isoda, Determination of Parameters of Electron Transport in Dye-Sensitized Solar Cells Using Electrochemical Impedance Spectroscopy, The Journal of Physical Chemistry B, 110 (2006) 13872-13880.

[67] A.S. Hart, C.B. K. C, N.K. Subbaiyan, P.A. Karr, F. D'Souza, Phenothiazine-Sensitized Organic Solar Cells: Effect of Dye Anchor Group Positioning on the Cell Performance, ACS Applied Materials & Interfaces, 4 (2012) 5813-5820.

Tables, schemes and figures captions

Table 1. Key CV patterns for the investigated molecules: reduction and oxidation peak potentials (E_{pc} and E_{pa} respectively), referred to the $Fc^+|Fc$ redox couple; for first reduction and oxidation peaks only: $dE_p/d\log v$ slopes; current densities j (normalized for concentration c and square root of potential scan rate $v^{0.5)}$; formal standard potentials $E°'$ (calculated as the average of $E_{p,forward}$ and $E_{p,backward}$); corresponding HOMO and LUMO energy levels together with the corresponding energy gap E_g.

Table 2. [a] N_2-saturated MeOH-EtOH 4-1v/v solutions (CM= 2×10^{-5} Lmol^{-1}) at 298 K. Rate constants k_r and k_{nr} are calculated using the equations $k_r=\Phi L/\tau$ and $k_{nr}=(1-\Phi L)/\tau$, on the assumption that $\Phi_{ISC}=1$ (ISC=intersystem crossing). [b] Calcd. at λ_{abs}, MLCT. [c] In a frozen MeOH-EtOH 4-1v/v matrix at 77 K.

Table 3. Photovoltaic properties of DSSCs with **RuLomp** dyes.

Table 4. The calculated values of electric equivalent circuit elements for DSSCs with the **RuLomp** dyes.

Scheme 1. Synthetic route for *meta* and *para* isomers of ligands (*m-4* and *p*-**4**).

Scheme 2. Synthetic route for *ortho* isomer of ligand (*o*-**4**).

Scheme 3. Synthesis of isomeric Ru-complexes (**6**).

Scheme 4. The adsorption geometry of **RuLo** (a), **RuLm** (b) and **RuLp** (c) dyes on titania surface.

Figure 1. A synopsis of normalized CV patterns of the investigated complexes, at 0.2 V/s potential scan rate.

Figure 2. a) UV/Vis/NIR absorption; b) emission spectra in MeOH-EtOH 4-1 mixture at 298 K; c) 77 K photoluminescence emission in rigid glass matrix of MeOH-EtOH.

Figure 3. The IPCE action of **RuLomp** sensitized devices.

Figure 4. The J-V curves of **RuLomp** sensitized devices.

Figure 5. Nyquist plots of impedance spectra of DSSC devices based on **RuLomp** sensitized devices.

Table 1.

	E_{pIIIc} (V)	E_{pIIc} (V)	E_{pIc} (V)	$-dE_p$ dlogv^{-1}	$jcv^{-0.5}$ (Acm^{-2}mol^{-1}dm^{3}V$^{-0.5}$s$^{0.5}$)	E_{pIa} (V) (*)	$dE_p/$ dlog$v$	$jcv^{-0.5}$ (Acm^{-2}mol^{-1}dm^{3}V$^{-0.5}$s$^{0.5}$)	$E^{\circ'}{}_{,Ic}$ (V)	$E^{\circ'}{}_{,Ia}$ (V)	E_{LUMO} (eV)	E_{HOMO} (eV)	E_g (eV)
Ru(bpy)$_3$Cl$_2$	-2.19	-1.95	-1.76	0.006	0.70	0.90			-1.70	0.88	-3.10	-5.68	2.58
455 2PF$_6$	-1.71 -2.02	-1.61	-1.19	0.040	0.21	1.02	0.005	0.65	-1.16	0.99	-3.64	-5.79	2.15
RuLo	-2.17	-1.94	-1.49	0.042	0.33	0.98	0.002	0.66	-1.47	0.95	-3.33	-5.75	2.42
RuLm	-2.17	-1.93	-1.69	0.003	0.76	0.93	0.003	0.68	-1.65	0.89	-3.15	-5.69	2.54
RuLp	-2.08	-1.94	-1.66		0.77	0.95	0.003	0.76	-1.58	0.92	-3.22	-5.72	2.50
B1	-2.23	-1.86	-1.67	0.002		0.94	0.000	0.87	-1.62	0.89	-3.19	-5.69	2.51

(*) Excluding the peak corresponding to Cl$^-$

Table 2.

	Temp	λ_{abs} (ε [x 10^4 Lmol^{-1}cm^{-1}]) [nm]	λ_{em} (FWHM[cm^{-1}]) [nm]	Φ_L N$_2$/(air)	τ [μs] N$_2$/(air)	k_r (s^{-1})	k_{nr} (s^{-1})
RuLo	RT	475(1.97), 329(3.41), 287(7.95), 245(5.80)	670 (2620)	0.095 (0.017)	1.90 (0.343)	$5.0*10^4$	$47.63*10^4$
	77K	567, 487, 338, 313, 293	646 (vibr. 1110cm^{-1}; S=0.52)		6.28		
RuLm	RT	459(2.02), 329(3.54), 288(7.70), 244(3.87)	633 (2680)	0.18 (0.033)	1.89 (0.352)	$9.52*10^4$	$43.39*10^4$
	RT+TFA	459, 323, 288	639 (2510)	0.172	1.78	$9.66*10^4$	$46.52*10^4$
	77K	459, 327, 292	611 (vibr. 1330cm^{-1}; S=0.56)		6.44		
RuLp	RT	460(1.97), 330(3.60), 287 (7.98), 245(3.59)	635 (2720)	0.19 (0.041)	1.97 (0.426)	$9.64*10^4$	$41.11*10^4$
	77K	459, 332	615 (vibr. 1400cm^{-1}; S=0.54)		7.0		

Table 3.

	Jsc (mAcm^{-2})	Voc (mV)	FF (%)	η (%)	N$_{dye}$ (10^{-7}molcm^{-2})
RuLo	0.76	534	55.6	0.22	0.73
RuLm	1.39	518	58.0	0.42	4.84
RuLp	2.28	560	63.0	0.80	5.61

Table 4.

	R1 (Ω)	R2 (Ω)	CPE1 ($10^{-5}\Omega^{-1}cm^{-2}s^n$)	R3 (Ω)	CPE2 ($10^{-5}\Omega^{-1}cm^{-2}s^n$)
RuLo	15.7	15.0	1.36	1237.0	5.22
RuLm	17.7	62.1	0.65	1076.0	1.11
RuLp	19.2	33.9	4.07	356.2	2.61
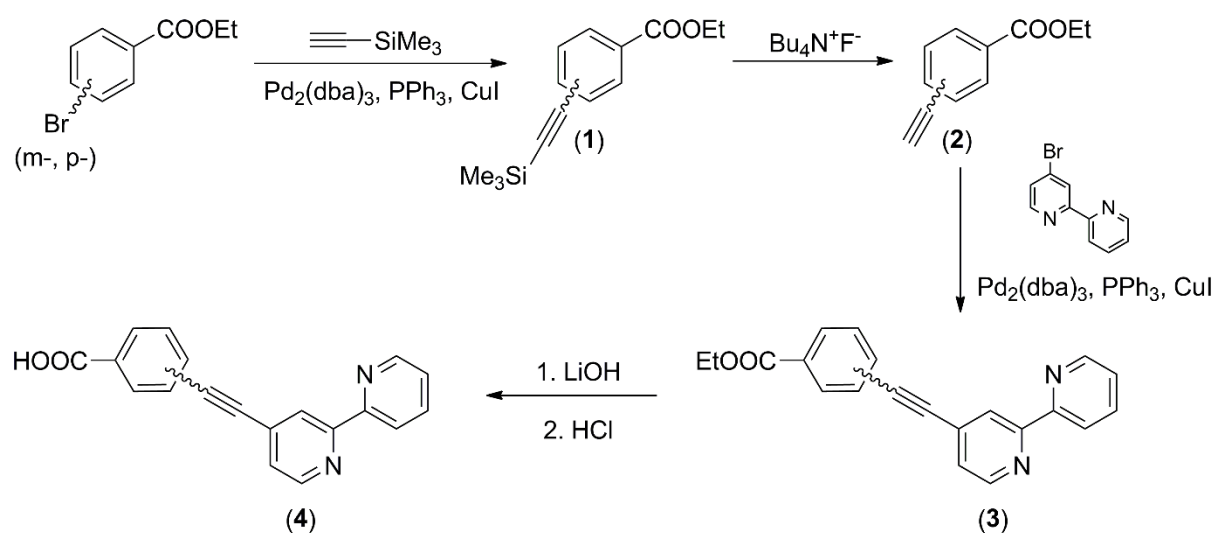
Scheme 1.
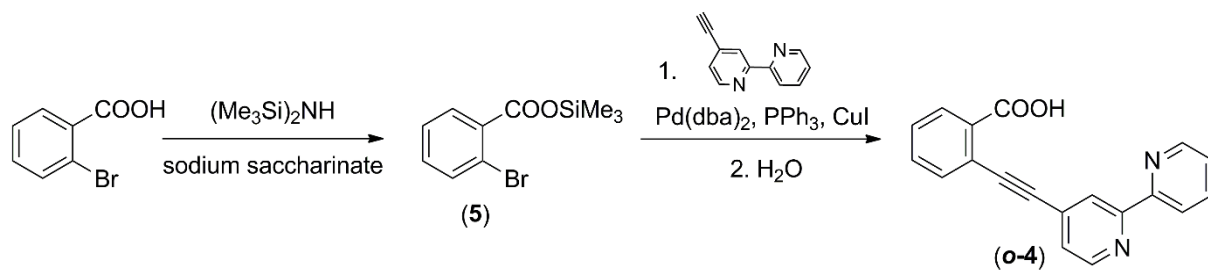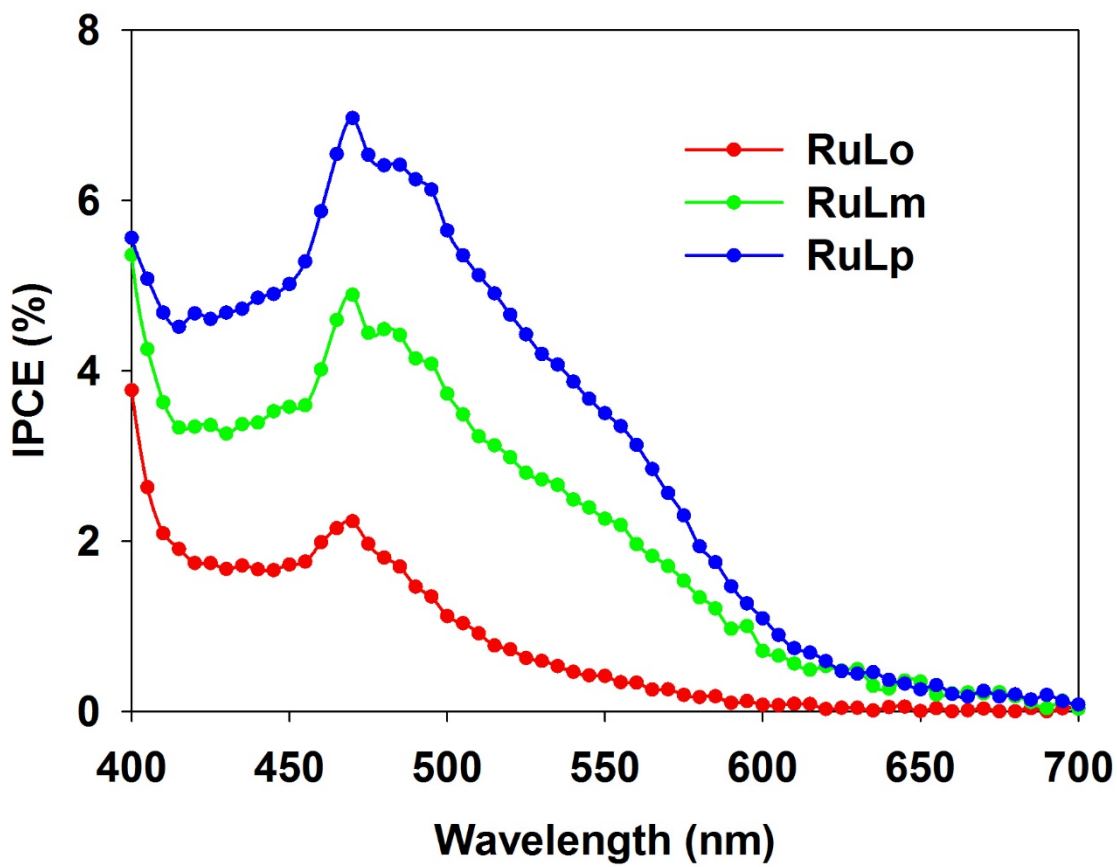
Scheme 2.
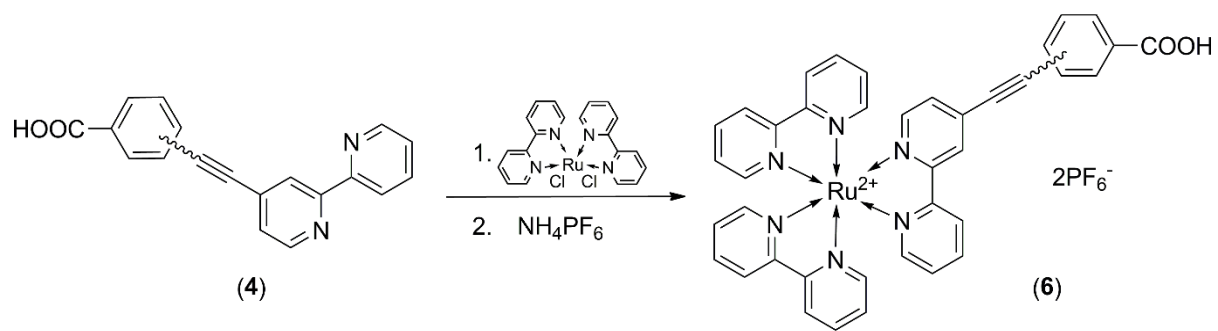
Scheme 3.
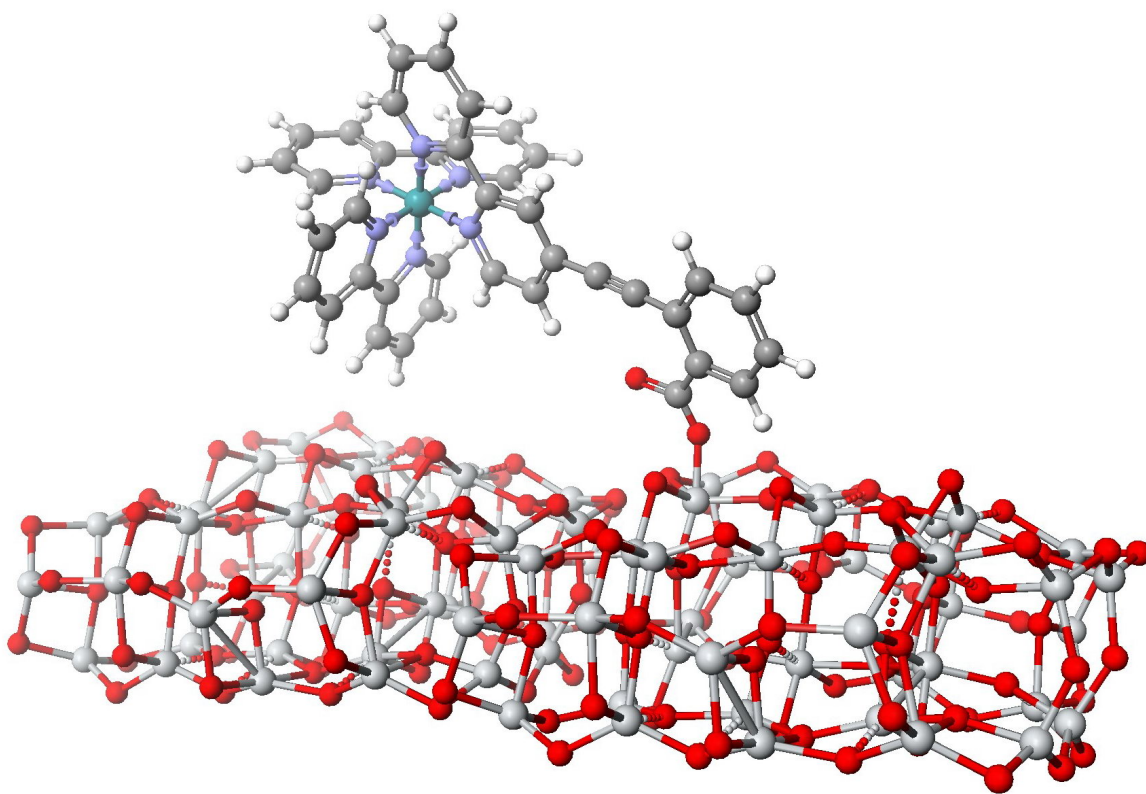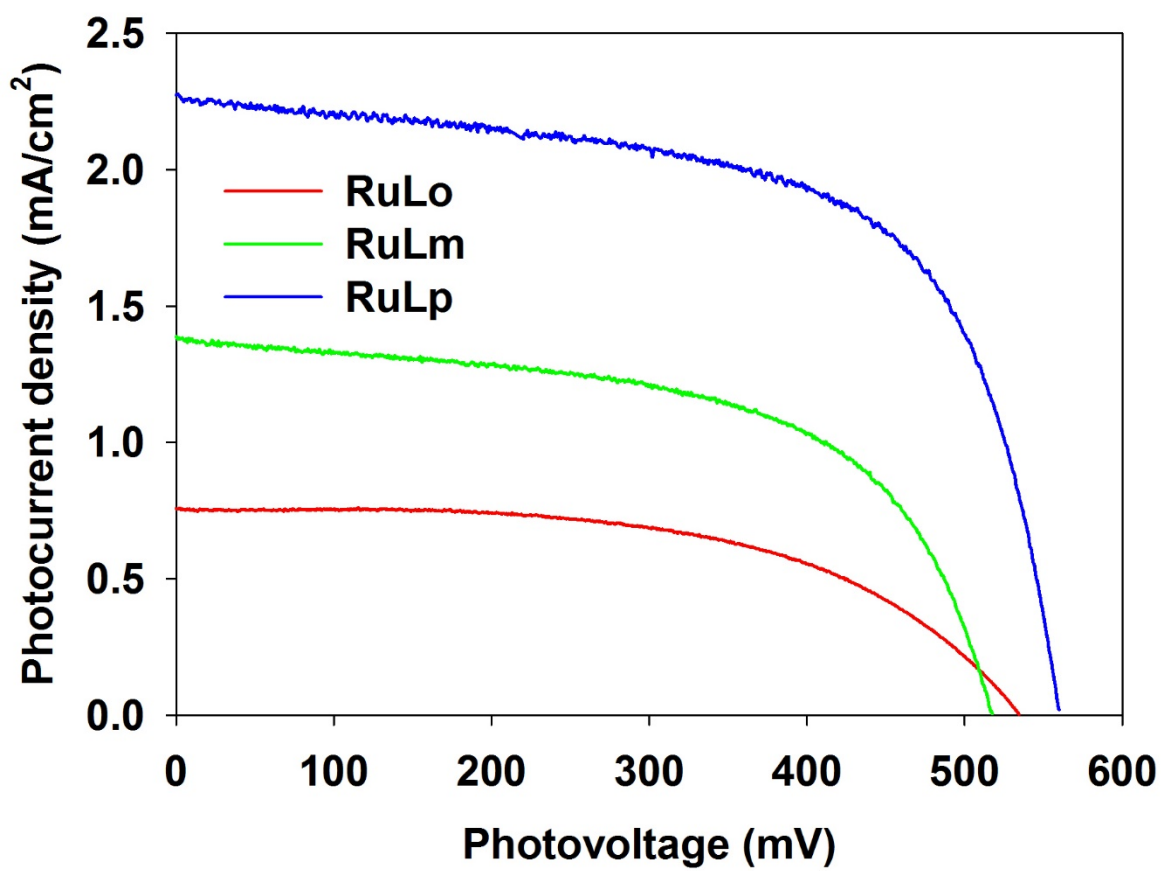
Scheme 4a.
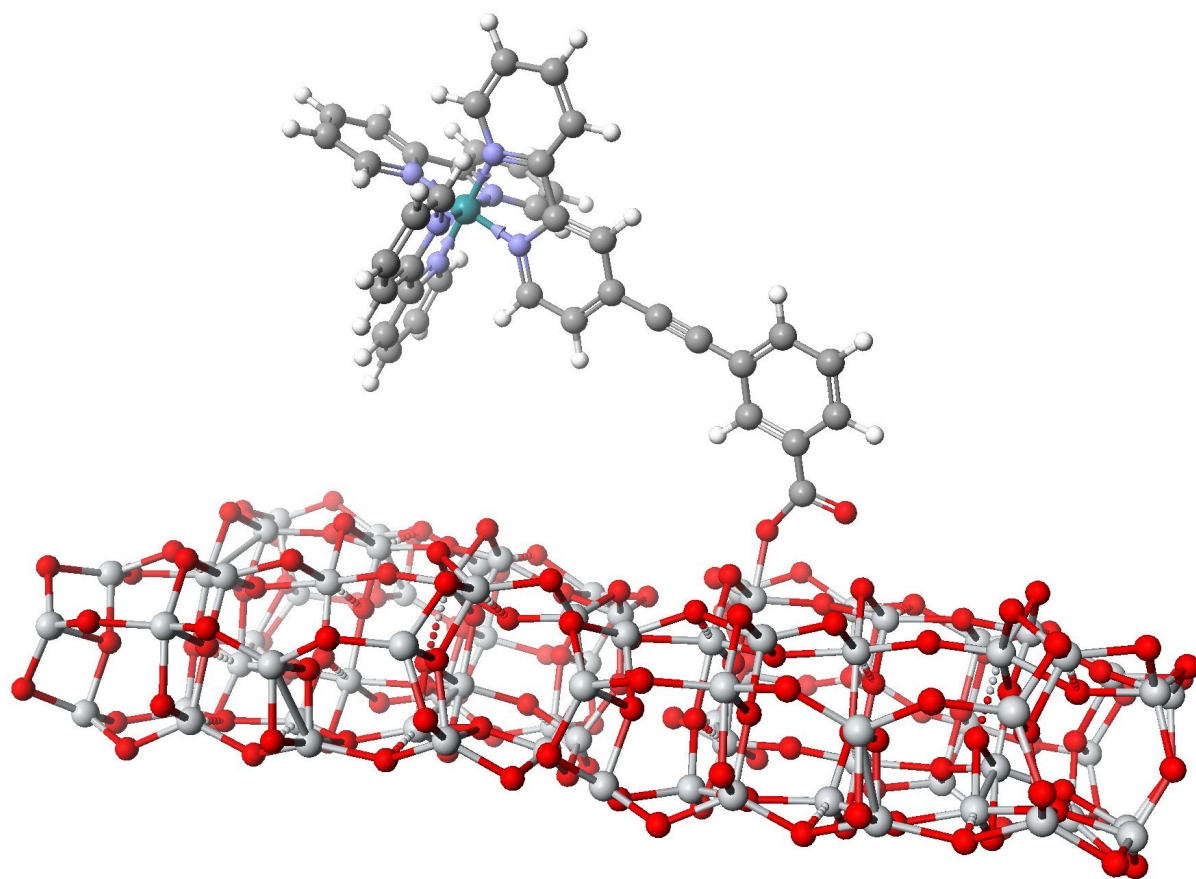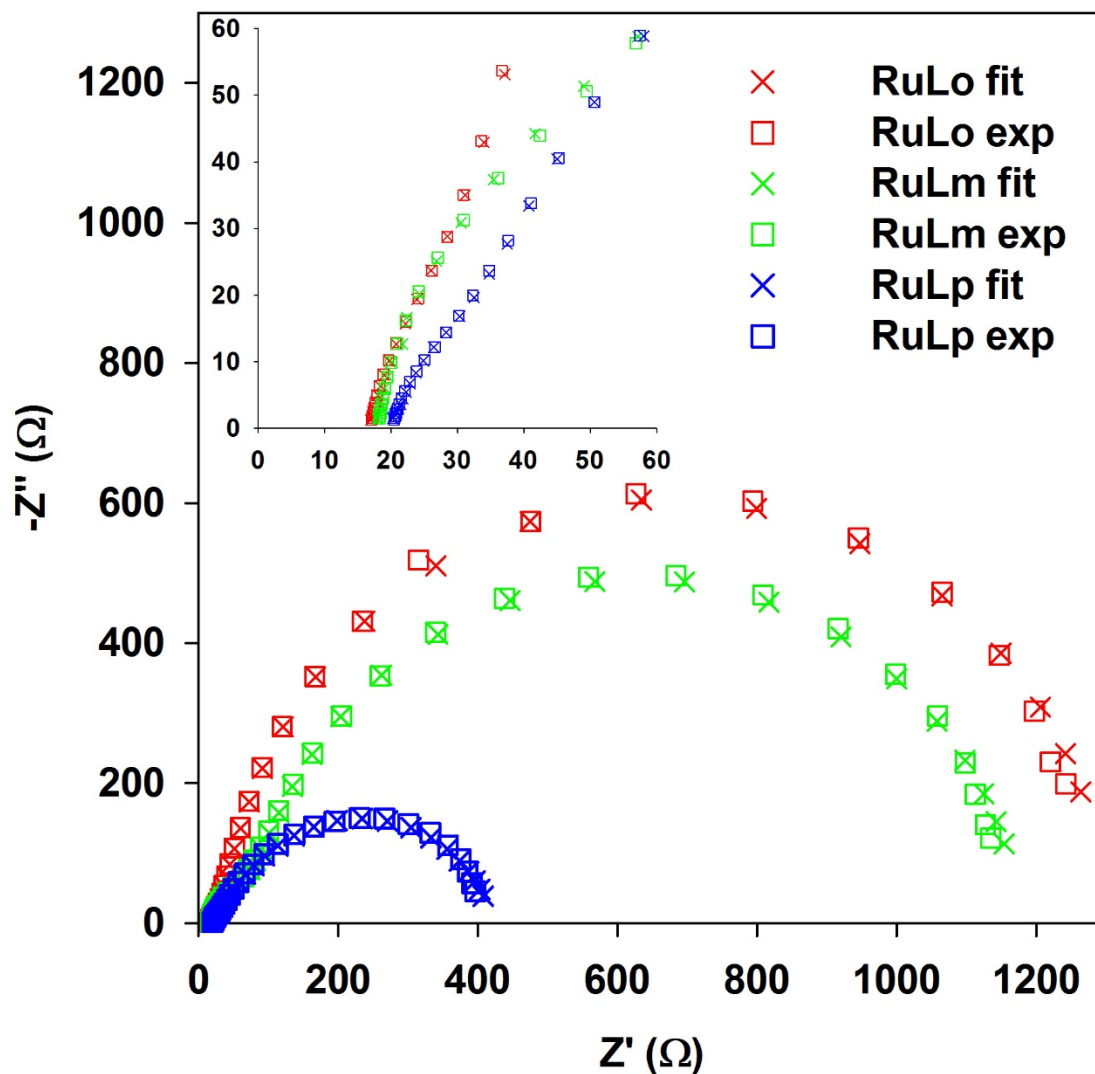
Scheme 4b.
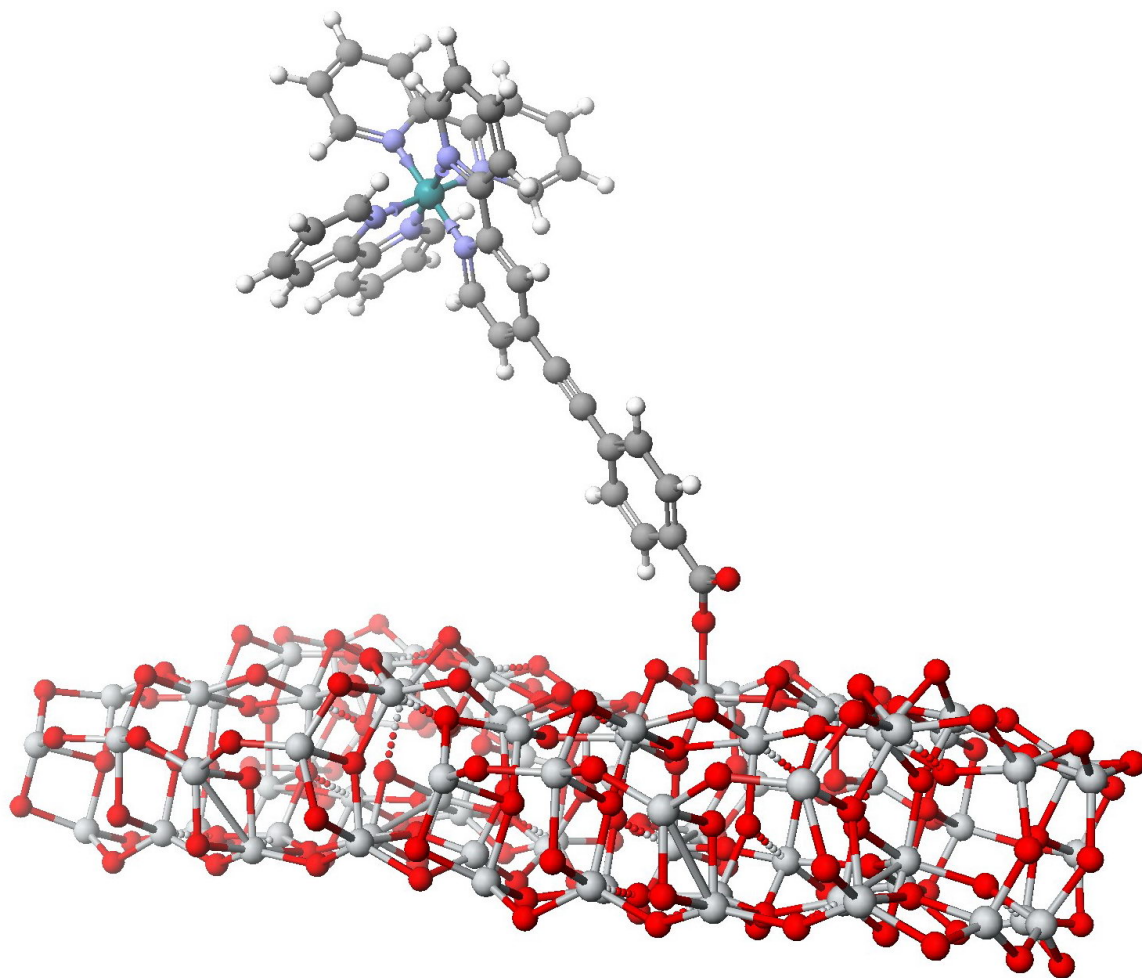
Scheme 4c.
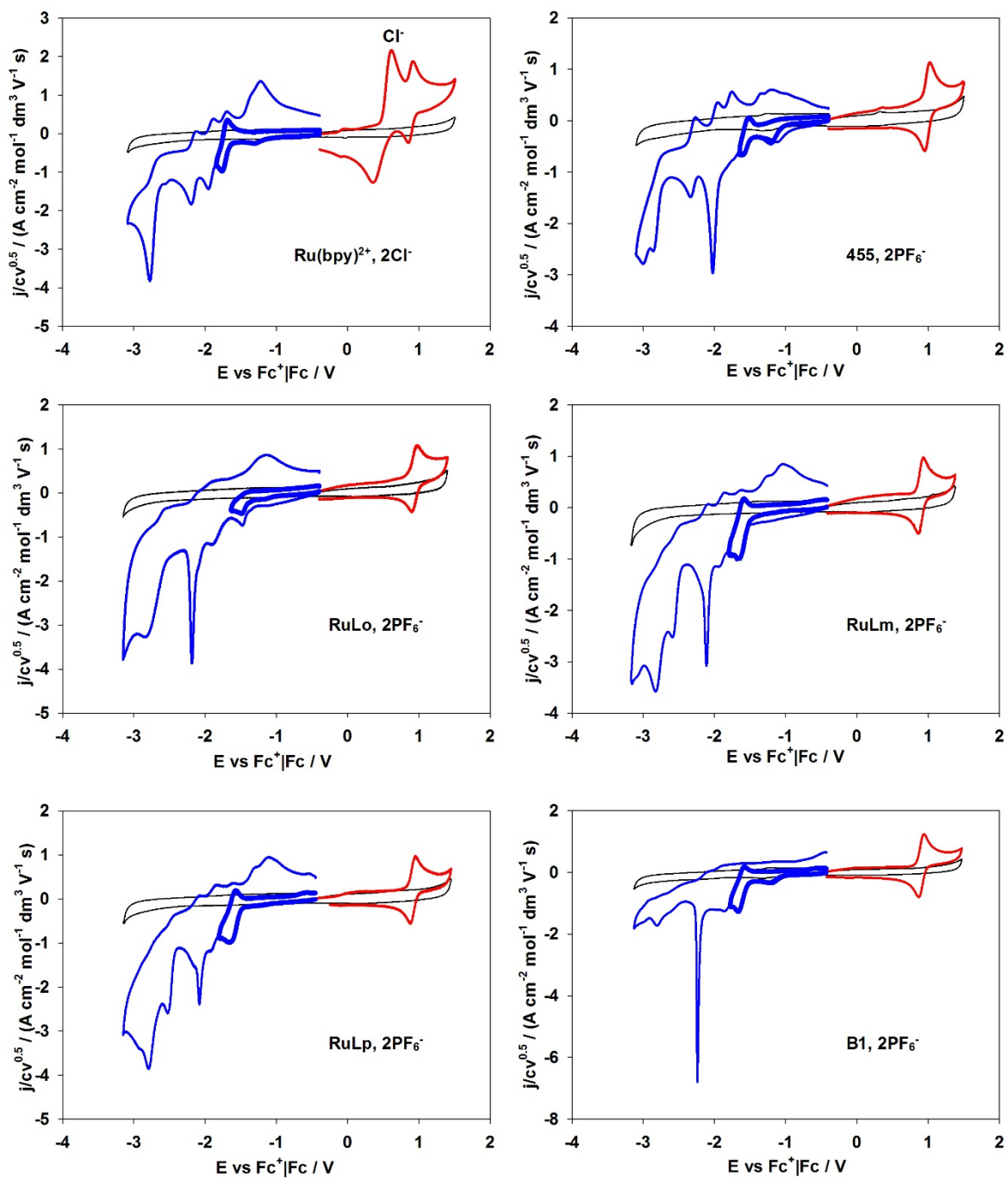
Figure 1.
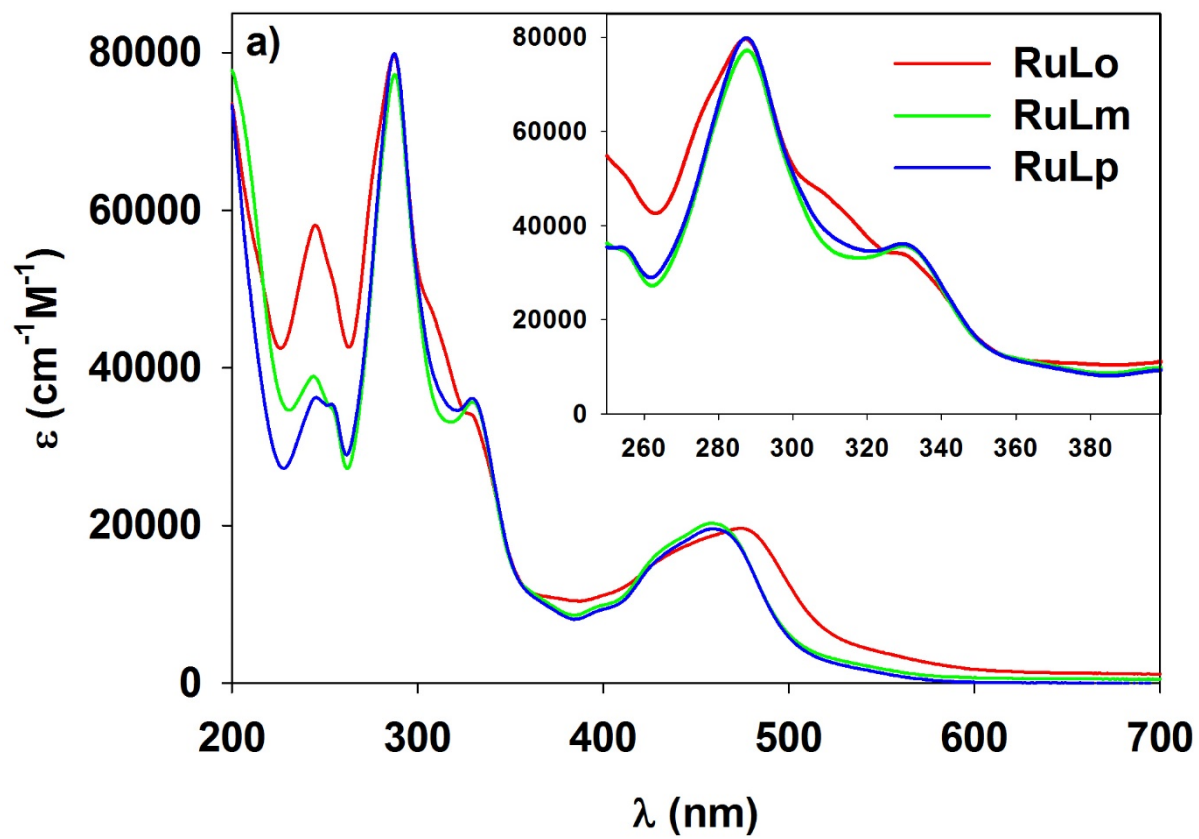
Fig 2a.
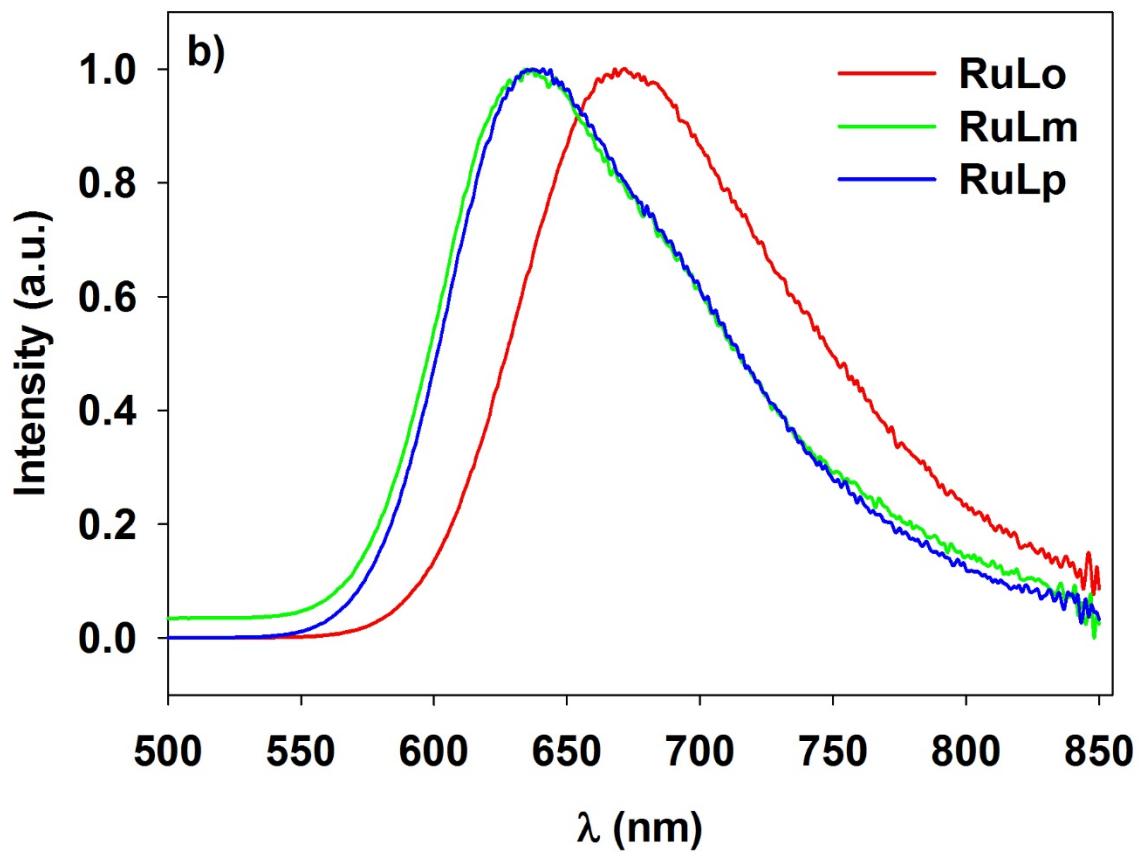
Figure 2b.
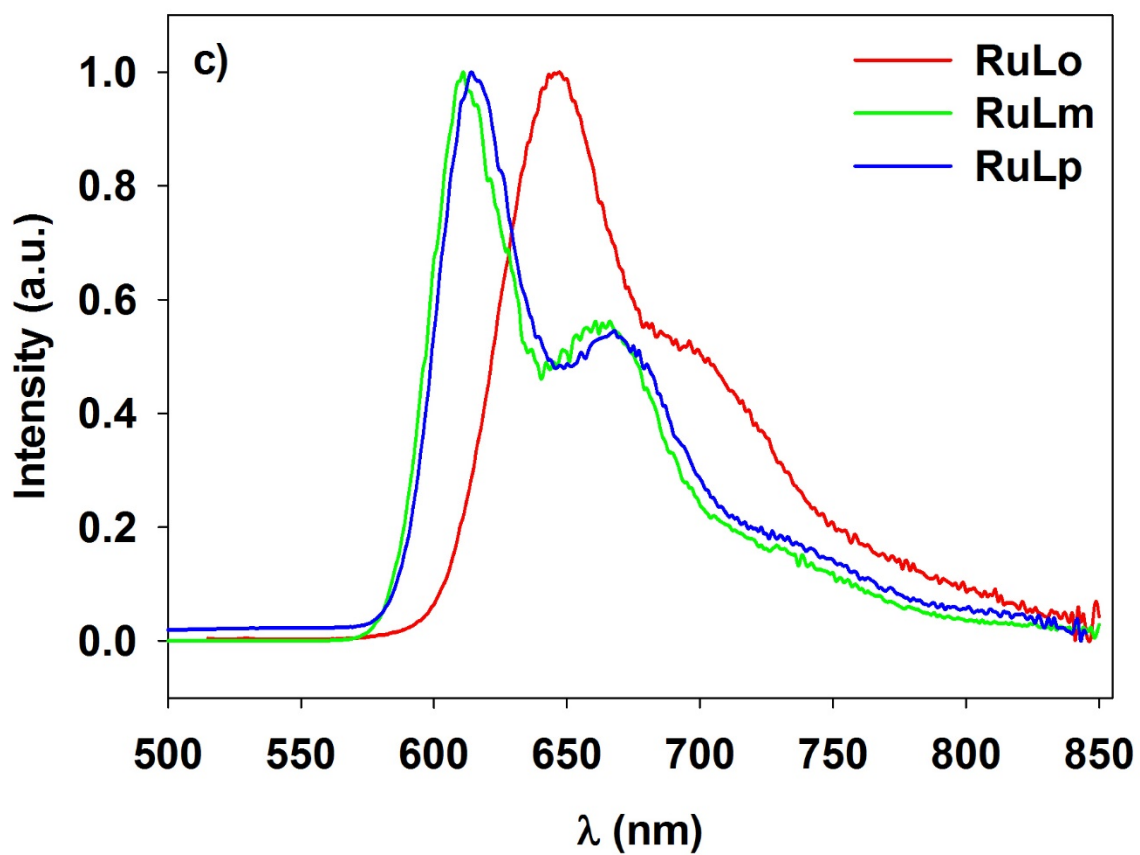
Figure 2c.

Figure 3.

Figure 4.

Figure 5.